2021

IMPROVING THE TEMPORAL ACCURACY OF TURBULENCE MODELS AND RESOLVING THE IMPLEMENTATION ISSUES OF FLUID FLOW MODELING

Kyle J. Schwiebert
Michigan Technological University, kjschwie@mtu.edu

IMPROVING THE TEMPORAL ACCURACY OF TURBULENCE MODELS AND RESOLVING THE IMPLEMENTATION ISSUES OF FLUID FLOW MODELING

By

Kyle J. Schwiebert

A THESIS

Submitted in partial fulfillment of the requirements for the degree of

MASTER OF SCIENCE

In Mathematical Sciences

MICHIGAN TECHNOLOGICAL UNIVERSITY

2021

This thesis has been approved in partial fulfillment of the requirements for the Degree of MASTER OF SCIENCE in Mathematical Sciences.

Department of Mathematical Sciences

Thesis Advisor:	*Dr. Alexander Labovsky*
Committee Member:	*Dr. Jiguang Sun*
Committee Member:	*Dr. Zhengfu Xu*
Department Chair:	*Dr. Jiguang Sun*

Dedication

To my wife and parents

without whose love and support this work and its creator would not be what they are today.

Contents

List of Figures

List of Tables

Acknowledgments

Portions of this thesis, including figures, have been submitted/published in peer-reviewed journals and are reproduced here in accord with the author-journal copyright agreement.

Abstract

A sizeable proportion of the work in this thesis focuses on a new turbulence model, dubbed ADC (the approximate deconvolution model with defect correction). The ADC is improved upon using spectral deferred correction, a means of constructing a higher order ODE solver. Since both the ADC and SDC are based on a predictor-corrector approach, SDC is incorporated with essentially no additional computational cost. We will show theoretically and using numerical tests that the new scheme is indeed higher order in time than the original, and that the benefits of defect correction, on which the ADC is based, are preserved.

The final two chapters in this thesis focus on a two important numerical difficulties arising in fluid flow modeling: poor mass-conservation and possible non-physical oscillations. We show that grad-div stabilization, previously assumed to have no affect on the target quantities of the test problem used, can significantly alter the results even on standard benchmark problems. We also propose a work-around and verify numerically that it has promise. Then we investigate two different formulations of Crank-Nicolson for the Navier-Stokes equations. The most attractive implementation, second order accurate for both velocity and pressure, is shown to introduce non-physical oscillations. We then propose two options which are shown to avoid the poor behavior.

Chapter 1

Notational Preliminaries and Background

1.1 Overview

Computational fluid dynamics (CFD) in general, and turbulence modeling in particular, remains a vibrant field with many more questions than answers. Recent work has shown that defect correction, often dismissed by turbulence modeling researchers, is computationally efficient in an "accuracy per unit time" sense for these problems. Especially in a world where improvements in computational resources come increasingly from higher numbers of processors rather than faster processors, the inherent

parallelizability of defect correction models make them attractive.

The most significant work in this thesis focuses on just one of these new models, dubbed ADC (the approximate deconvolution model with defect correction). The ADC is improved upon using spectral deferred correction (SDC). SDC is a well-known method for constructing high-order ODE solvers. Since both methods require a two step process, and through the method of lines the time-dependent Navier-Stokes equations produce a system of ODEs, incorporating SDC into the ADC is a natural extension. We will show theoretically and using numerical tests that the new scheme is indeed higher order than the original, and that the benefit of defect correction is preserved.

The final two chapters in this thesis focus on a two important numerical difficulties: poor mass-conservation and possible non-physical oscillations. The most widely used methods for 2D incompressible flow often struggle to adhere to the incompressibility condition. First we will investigate grad-div stabilization, the overwhelmingly popular choice for improving the mass conservation of a solution. We show that grad-div stabilization, previously assumed to have no affect on the target quantities of the test problem used, can significantly alter the results even on standard benchmark problems. We also propose a work-around and briefly verify numerically that it is worth further investigation.

In the final chapter we investigate two different formulations of Crank-Nicolson for the

Navier-Stokes equations (NSE). We will show that care must be taken to avoid non-physical oscillatory behavior. Although the non-physical oscillations often present in Crank-Nicolson schemes are well-known to applied and computational mathematicians, the effect is often ignored in the CFD community. Chapter 4 argues that this may not always be the correct approach.

1.2 The Incompressible Navier-Stokes Equations

Consider the NSE for an incompressible fluid flow in $\Omega \in \mathbb{R}^d$: find the velocity-pressure pair $u : \Omega \times [0,T] \ \rightarrow \mathbb{R}^d \, (d = 2,3)$ and $p : \Omega \times (0,T] \rightarrow \mathbb{R}$ satisfying

$$
\begin{aligned}
& u_t + u \cdot \nabla u - \nu \Delta u + \nabla p = f, \ \text{for } x \ \in \ \Omega, \, 0 < t \leq T \\
& \nabla \cdot u = 0, \ x \ \in \ \Omega, \ \text{for } 0 \leq t \leq T, \\
& u(x,0) = u_0(x), \ \text{for } x \ \in \ \Omega,
\end{aligned}
\tag{1.2.1}
$$

with normalization condition $\int_\Omega p(x,t) \, dx = 0$ for $0 < t \leq T$. In Chapter 2, we will assume zero periodic boundary conditions for simplicity of the error analysis. We do this although various test problems, namely that which is the focus of Chapters 3 and 4, will require that we impose Dirichlet boundary conditions.

We may also wish to define the weak form of the NSE. First we define the appropriate velocity and pressure spaces:

$$X = \{v \in (L^2(\Omega))^2 : \nabla v \in (L^2(\Omega))^2, v|_{\partial\Omega} = 0\}$$
$$Q = \{q \in L^2(\Omega) : \int_\Omega p(x,t)\ dx = 0\}$$

Let $(\cdot,\cdot)$ represent the usual $L^2(\Omega)$ inner product. Now, consider the weak form of time-dependent incompressible NSE. Find $(u,p) \in (X,Q)$ such that for all $(u,p) \in (X,Q)$:

$$(u_t, v) + (u \cdot \nabla u \cdot v) - \nu(\nabla u, \nabla v) - (p, \nabla \cdot v) = (f, v)$$
$$(q, \nabla \cdot u) = 0 \tag{1.2.2}$$

1.3 2D Incompressible Flow around a Cylinder

Some of the follow work focuses on the test problem considered in [2]. Chapter 2 shows how important this problem is to turbulent flow research. Many test problems in turbulence modeling are qualitative in nature, however, this one is quantitative. Therefore, researchers often use this problem as a first task for a novel idea or model. Figure 1.1 shows the computational domain, with the flow direction being left to right, indicated by the arrow. Here the two-dimensional flow is considered in $\Omega =$

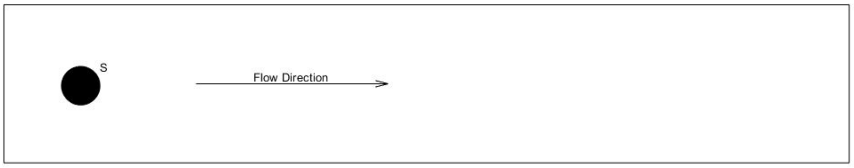

Figure 1.1: Domain of the Test Problem

$[0, 2.2] \times [0, 0.41]$ past a cylinder of radius 0.05, whose circumference is labeled S, centered at $(0.2, 0.2)$. Take the forcing term $f = 0$, viscosity $\nu = 0.001$, and final time $T = 8$.

$$\mathbf{u}(t; 0, y) = \mathbf{u}(t; 2.2, y) = \frac{1}{0.41^2} \sin(\pi t/8)(6y(0.41 - y), 0).$$

No-slip conditions are prescribed at the other boundaries.

The quantities of interest and their respective intervals as given in [3]: the maximal drag coefficient $c_{d,max}^{ref}(t)$, maximal lift coefficient $c_{l,max}^{ref}(t)$ and the pressure difference at the final time, $\Delta p^{ref}(8)$:

$$c_{d,max}^{ref}(t) \in [2.93, 2.97], \qquad c_{l,max}^{ref}(t) \in [0.47, 0.49], \qquad \Delta p^{ref}(8) \in [-0.115, -0.105].$$

To a lesser extent, we may concern ourselves with when the maximal drag and lift coefficents occur. Again from [3], we have:

$$t(c_{d,max}^{ref}) \in [3.93, 3.94], \qquad t(c_{l,max}^{ref}) = 5.72.$$

Chapter 2

Higher Temporal Accuracy For LES-C Turbulence Models

2.1 Introduction

In many physical, astrophysical and engineering applications the low viscosity fluid flows enter the so-called turbulence regime, characterized by sporadic changes in velocity and pressure. These flows cannot be modeled by direct numerical simulation (DNS), as various failure modes are documented in the literature: the iterative solvers fail to converge within the time frame of the problem, and the mesh size, required to capture the correct qualitative behavior of the true solution, is prohibitively small. To

grapple with these issues, turbulence models have been developed. One commonly used family of turbulence models, Large Eddy Simulations (LES), is based on the idea that the flow can be represented by a collection of scales with different sizes, and instead of trying to approximate all of them down to the smallest one, one defines a filter width $\delta > 0$ and computes only the scales of size bigger than δ (large scales), whereas the effect of the small scales on the large scales is modeled. This aims at reducing the number of degrees of freedom in a simulation while accurately representing the large structures in the flow.

Different LES models seek to approximate different quantities of interest (QoI). These may be the velocity-pressure pair (u, p), the filtered pair $(\bar{u}, \bar{p})$, or a combination of the above. A method was proposed in [1], where any LES model could be combined with a defect correction method (of predictor-corrector type) to produce a solution that is more accurate than the LES solution computed on the same spatial mesh. Alternatively, the new method could be viewed as getting to within the desired tolerance faster, on a coarser mesh.

The LES-C (Large Eddy Simulation with Correction) turbulence models were introduced in [1] to reduce the LES modeling error via the following procedure.

Algorithm 2.1.1 *Turbulence Modeling with Correction.*

1. If needed, rewrite the NSE system so that the velocity-pressure pair (u, p) is transformed into the QoI pair $(h(u), g(p))$:

$$\widetilde{NSE}(QoI) = 0.$$

2. Using the turbulence model (TM), find the defect step approximation of the QoI:

$$TM(w_1, q_1) = 0.$$

3. The correction step provides a more accurate approximation of the QoI, via

$$TM(w_2, q_2) = TM(w_1, q_1) - \widetilde{NSE}(w_1, q_1).$$

When constructing an LES-C model via Algorithm 2.1.1, one can aim at reducing not only the modeling error, but also the error due to temporal discretization. In order to keep the computational cost unchanged, the reduction of the temporal discretization error has to be done within the predictor-corrector framework of Algorithm 2.1.1. The corresponding idea would fall into the category of "deferred correction" methods - a term introduced by Dutt, Greengard and Rokhlin, [4], for the defect correction in ODEs. These methods were further developed by Minion et al., [5, 6].

The deferred correction approach to ODEs is based on replacing the original ODE with the corresponding Picard integral equation, discretizing the time interval, solving the integral equation approximately and then correcting the solution by solving a sequence of error equations on the same grid with the same scheme; see [4] for the detailed mathematical presentation of these methods. The so-called spectral deferred correction (SDC) method within the deferred correction framework was developed in [5].

Deferred correction has already been successfully used in turbulence modeling to improve temporal accuracy - see, e.g., [7, 8]. In recent years several papers have been published, that successfully applied deferred correction to fluid flows in various settings, [9, 10, 11, 12, 13]. Given that a LES-C model already requires the correction step, it seems natural to try and incorporate deferred correction into this step, so that extra temporal accuracy is achieved at almost no extra computational cost.

In the authors' opinion, it is important to understand the benefits of deferred correction, so that the expectations and objectives are clear from the beginning. As a method that provides increased accuracy, deferred correction has been compared to the other well known higher accuracy families: see, e.g., [5] for the comparison of this technique against the BDF and Runge-Kutta methods. However, there are also other advantages of the deferred correction, that could be crucial in computationally expensive applications of turbulent fluid flows, or flows in complex geometries. One

particular setting, where deferred correction was proven to be helpful, was described in [10]: when trying to decouple a fluid-fluid interaction problem with nonlinear interface condition, most of the well known time discretization methods became unstable. A clever way to introduce a partitioned method was proposed in [14], but it was only first order accurate with respect to the time step. Deferred correction came to the rescue, allowing for the increased time accuracy, while keeping the method partitioned and unconditionally stable, [10].

Another important benefit of this technique is that it could be built on virtually any lower order accurate method: the user decides, which method for time discretization should be used in the defect step, based on the extra stability or other desirable features. The deferred correction is then used to ensure that the accuracy is improved in the correction step. In this chapter the Backward Euler method will be used in the defect step, and the deferred correction would increase the accuracy from first to second order in the correction step. Since the LES-C models already employ the correction step to reduce the modeling error, deferred correction could be added to improve the accuracy of any underlying time discretization method for no extra computational cost.

The remainder of this chapter is organized as follows. section 2.2 introduces the necessary notation; the new model is then introduced and full numerical analysis is done in section 2.3. Given the skepticism, that is sometimes displayed in the CFD

community towards the defect correction methods for fluid flows (and stiff problems in general), it is important to provide various numerical tests to demonstrate the method's efficiency; this is done in section 4.2. There, the claimed convergence rates are verified on a problem with known true solution; this is followed by two more famous benchmark problems, flows past a step and the computation of drag and lift coefficients past a circular obstacle, where the correction step is clearly shown to provide more accurate results, even on a coarse mesh.

2.2 Notation and Preliminaries

Throughout the chapter, the norm $\|\cdot\|$ denotes the usual $L^2(\Omega)$-norm of scalars, vectors, and tensors, induced by the usual L^2 inner-product.

The space that the velocity (at time t) belongs to is given by

$$X = H^1_{per}(\Omega)^d = \{v \in L^2(\Omega)^d : \nabla v \in L^2(\Omega)^{d\times d} \text{ and } v \text{ is periodic with period } L\}$$

equipped with the norm $\|v\|_X = \|\nabla v\|$. The space dual to X is equipped with the

norm

$$\|f\|_{-1} = \sup_{v \in X} \frac{(f, v)}{\|\nabla v\|}.$$

The pressure (at time t) is sought in the space

$$Q = L^2_{per}(\Omega) = \{q : q \in L^2(\Omega), \int_\Omega q(x)dx = 0, q \text{ periodic with period } L\}.$$

Also introduce the space of weakly divergence-free functions

$$V = \{v \in X : (\nabla \cdot v, q) = 0, \forall q \in Q\}.$$

For measurable $v : [0, T] \to X$, define

$$\|v\|_{L^p(0,T;X)} = (\int_0^T \|v(t)\|_X^p dt)^{\frac{1}{p}}, \ 1 \leq p < \infty$$

and

$$\|v\|_{L^\infty(0,T;X)} = \operatorname{ess}\sup_{0\le t\le T} \|v(t)\|_X.$$

Define the trilinear form on $X \times X \times X$

$$b(u,v,w) = \int_\Omega u \cdot \nabla v \cdot w dx.$$

Throughout the chapter, we shall assume that the velocity-pressure finite element spaces $X^h \subset X$ and $Q^h \subset Q$ are conforming and satisfy the discrete inf-sup, or LBB^h, condition. One of the most commonly used choices is the Taylor-Hood (P_2, P_1) pair of piecewise quadratic polynomials for the velocity and piecewise linears for the pressure.

The idea of approximate deconvolution modeling is based on the definition and properties of the following operator.

Definition 1 (Approximate Deconvolution Operator) *For a fixed finite N, define the Nth approximate deconvolution operator G_N by*

$$G_N\phi = \sum_{n=0}^{N} (I - A^{-1})^n \phi,$$

where the averaging operator A^{-1} is the differential filter: given $\phi \in L^2(\Omega)$, $\overline{\phi}^{\delta} \in H^2(\Omega)$ is the unique solution of

$$A\overline{\phi}^{\delta} := -\delta^2 \Delta \overline{\phi}^{\delta} + \overline{\phi}^{\delta} = \phi \quad \text{in } \Omega, \tag{2.2.1}$$

subject to periodic boundary conditions. Under periodic boundary conditions, this averaging operator commutes with differentiation.

Throughout the chapter, the filtered (averaged) solution $\bar{u}$ will be used. If u is the velocity field that solves the NSE, then, given the filtering width δ, $\bar{u}$ is defined via $A\bar{u} = u$.

Lemma 1 *The operator G_N is compact, positive, and is an asymptotic inverse to the filter A^{-1}, i.e., for very smooth ϕ and as $\delta \to 0$, it satisfies*

$$\phi = G_N \overline{\phi}^{\delta} + (-1)^{N+1} \delta^{2N+2} \Delta^{N+1} A^{-(N+1)} \phi. \tag{2.2.2}$$

The proof of Lemma 1 can be found in [15].

Define the explicitly skew-symmetrized trilinear form

$$b^*(u, v, w) := \frac{1}{2}(u \cdot \nabla v, w) - \frac{1}{2}(u \cdot \nabla w, v).$$

The following estimate is easy to prove; see, e.g., [16]: there exists a constant $C = C(\Omega)$ such that

$$|b^*(u,v,w)| \leq C(\Omega)\|\nabla u\|\|\nabla v\|\|\nabla w\|. \tag{2.2.3}$$

The proofs will also require a sharper bound on the nonlinearity. This upper bound is improvable in $\mathbb{R}^2$.

Lemma 2 (Sharper bound on the nonlinear term) *Let $\Omega \subset \mathbb{R}^d$, $d = 2, 3$. For all $u, v, w \in X$*

$$|b^*(u,v,w)| \leq C(\Omega)\sqrt{\|u\|\|\nabla u\|}\|\nabla v\|\|\nabla w\|.$$

For a proof, please refer to [16].

We also define the following norm, induced by the deconvolution operator A:

$$\|\phi\|_A^2 = \|\phi\|^2 + \delta^2\|\nabla\phi\|^2.$$

The following discrete Gronwall's lemma (see, e.g., [17]) will be utilized in the subsequent analysis.

Lemma 3 *(Gronwall's lemma) Let k, M, and $a_\mu, b_\mu, c_\mu, \gamma_\mu$, for integers $\mu > 0$, be nonnegative numbers such that*

$$a_n + k\sum_{\mu=0}^{n} b_\mu \leq k\sum_{\mu=0}^{n} \gamma_\mu a_\mu + k\sum_{\mu=0}^{n} c_\mu + M \text{ for } n \geq 0. \tag{2.2.4}$$

Suppose that $k\gamma_\mu < 1$, for all μ, and set $\sigma_\mu \equiv (1 - k\gamma_\mu)^{-1}$. Then,

$$a_n + k\sum_{\mu=0}^{n} b_\mu \leq exp\left(k\sum_{\mu=0}^{n} \sigma_\mu\gamma_\mu\right)\left\{k\sum_{\mu=0}^{n} c_\mu + M\right\} \text{ for } n \geq 0. \tag{2.2.5}$$

The following constants and assumptions on the problem data (written here as assumptions on the true solution u) will be used in the proofs below.

Definition 2

$$C_{\bar{u}} := \|\bar{u}(x,t)\|_{L^\infty(0,T;L^\infty(\Omega))}$$

$$C_{\nabla\bar{u}} := \|\nabla\bar{u}(x,t)\|_{L^\infty(0,T;L^\infty(\Omega))}$$

$$C_{\zeta} := \|\zeta(x,t)\|_{L^\infty(0,T;L^\infty(\Omega))}$$

$$C_{\nabla\zeta} := \|\nabla\zeta(x,t)\|_{L^\infty(0,T;L^\infty(\Omega))}$$

2.3 ADC - Approximate Deconvolution with Correction

One member of the newly proposed family of LES-C models was discussed in [1] - the Approximate Deconvolution with Correction (ADC) model. Implementing the defect correction procedure to reduce the modeling error of the underlying Approximate Deconvolution Model (ADM), the ADC seeks two consequent approximations to the true solution $(\bar{u}, p)$ via the following equations.

Consider the semidiscrete (continuous in time, discretized in space using Galerkin finite element method) case. The ADM is used as the first step of ADC: find $(w_1, \zeta_1, q_1) \in (X^h, X^h, Q^h)$ such that for any $(v^h, \xi^h, \chi^h) \in (X^h, X^h, Q^h)$

$$
\begin{aligned}
(w_{1,t}, v^h) + \delta^2(\nabla w_{1,t}, \nabla v^h) + \nu(\nabla w_1, \nabla v^h) + \nu\delta^2(\nabla \zeta_1, \nabla v^h) \qquad (2.3.1)\\
+b^*(w_1, w_1; v^h) - (q_1, \nabla \cdot v^h) = (f, v^h),\\
(\nabla w_1, \nabla \xi^h) = (\zeta_1, \xi^h),\\
(\nabla \cdot w_1, \chi^h) = 0,
\end{aligned}
$$

subject to $w_1(0,x) = \overline{u}_0^\delta(x)$ and periodic boundary conditions.

The correction step of the ADC reads: find $(w_2, \zeta_2, q_2) \in (X^h, X^h, Q^h)$ such that for any $(v^h, \xi^h, \chi^h) \in (X^h, X^h, Q^h)$

$$\begin{aligned}(w_{2,t}, v^h) + \delta^2(\nabla w_{2,t}, \nabla v^h) + \nu(\nabla w_2, \nabla v^h) + \nu\delta^2(\nabla \zeta_2, \nabla v^h) \\ +b^*(w_2, w_2; v^h) - (q_2, \nabla \cdot v^h) = (f, v^h) \\ -\delta^2 b^*(\zeta_1, w_1; v^h) - \delta^2 b^*(w_1, \zeta_1; v^h) - \delta^4 b^*(\zeta_1, \zeta_1; v^h), \\ (\nabla w_2, \nabla \xi^h) = (\zeta_2, \xi^h), \\ (\nabla \cdot w_2, \chi^h) = 0.\end{aligned} \tag{2.3.2}$$

2.3.1 New Model: ADC with Deferred Correction

When constructing an LES-C model via Algorithm 2.1.1, one can aim at reducing not only the modeling error, but also the error due to temporal discretization. We

propose the following model, which combines the ADC of [1] with a two-step deferred correction method. When based on the ADM with Backward Euler's temporal discretization, the new model reads: find $(w_1^{n+1}, \zeta_1^{n+1}, q_1^{n+1})$, $(w_2^{n+1}, \zeta_2^{n+1}, q_2^{n+1}) \in (X^h, X^h, Q^h), \forall (v^h, \xi^h, \chi^h) \in (X^h, X^h, Q^h)$ at $t = t_{n+1}$, $n \geq 0$, with $\Delta t := t_{i+1} - t_i$, satisfying

$$
\begin{aligned}
(\frac{w_1^{n+1} - w_1^n}{\Delta t}, v^h) + \delta^2(\frac{\nabla w_1^{n+1} - \nabla w_1^n}{\Delta t}, \nabla v^h) + \nu(\nabla w_1^{n+1}, \nabla v^h) \quad (2.3.3)\\
+\nu\delta^2(\nabla \zeta_1^{n+1}, \nabla v^h) + b^*(w_1^{n+1}, w_1^{n+1}; v^h) - (q_1^{n+1}, \nabla \cdot v^h) = (f(t_{n+1}), v^h),\\
(\nabla w_1^{n+1}, \nabla \xi^h) = (\zeta_1^{n+1}, \xi^h),\\
(\nabla \cdot w_1^{n+1}, \chi^h) = 0.
\end{aligned}
$$

$$
\begin{aligned}
(\frac{w_2^{n+1}-w_2^n}{\Delta t},v^h)+\delta^2(\frac{\nabla w_2^{n+1}-\nabla w_2^n}{\Delta t},\nabla v^h)+\nu(\nabla w_2^{n+1},\nabla v^h) \qquad (2.3.4)\\
+\nu\delta^2(\nabla\zeta_2^{n+1},\nabla v^h)+b^*(w_2^{n+1},w_2^{n+1};v^h)\\
-(q_2^{n+1},\nabla\cdot v^h)=(\frac{f(t_{n+1})+f(t_n)}{2},v^h)\\
+\frac{\Delta t}{2}\nu(\frac{\nabla w_1^{n+1}-\nabla w_1^n}{\Delta t},\nabla v^h)+\frac{\Delta t}{2}\nu\delta^2(\frac{\nabla\zeta_1^{n+1}-\nabla\zeta_1^n}{\Delta t},\nabla v^h)\\
+\frac{1}{2}b^*(w_1^{n+1},w_1^{n+1};v^h)-\frac{1}{2}b^*(w_1^n,w_1^n;v^h)-\frac{\Delta t}{2}(\frac{q_1^{n+1}-q_1^n}{\Delta t},\nabla\cdot v^h)\\
-\delta^2b^*(\zeta_1^{n+1},w_1^{n+1};v^h)-\delta^2b^*(w_1^{n+1},\zeta_1^{n+1};v^h)-\delta^4b^*(\zeta_1^{n+1},\zeta_1^{n+1};v^h),\\
(\nabla w_2^{n+1},\nabla\xi^h)=(\zeta_2^{n+1},\xi^h),\\
(\nabla\cdot w_2^{n+1},\chi^h)=0.
\end{aligned}
$$

Compared with the ADC model of [1], the model (2.3.3)-(2.3.4) starts with the same defect step. However, there are five more terms in the right hand side of (2.3.3) which would lead to increased temporal accuracy of this new model. This is done with essentially no extra cost, compared to the ADC, because the only modification concerns the change in the right hand side of the correction step, with the known quantity.

Stability and accuracy of the ADM model (2.3.3) are well-established - see, e.g., the following theorems from [7].

Theorem 1 (Stability of the first approximation) *Let w_1 satisfy (2.3.3). Let $f \in L^2(0,T;H^{-1}(\Omega))$. Then, for $n = 0, \ldots, N-1$,*

$$\|w_1^{n+1}\|_A^2 + \nu\Delta t\Sigma_{i=0}^n\|\nabla w_1^{i+1}\|^2 + \nu\delta^2\Delta t\Sigma_{i=0}^n\|\zeta_1^{i+1}\|^2 \leq \|w_1^0\|_A^2 + \frac{1}{\nu}\Delta t\Sigma_{i=0}^n\|f(t_{i+1})\|_{-1}^2.$$

Let C be a constant independent of $h, \Delta t, \Omega, \nu, f$, and suppose that the finite element spaces X^h, Q^h consist of continuous piecewise polynomials of degree m and $m-1$, respectively (e.g., $m = 2$ corresponds to Taylor-Hood elements).

Theorem 2 (Accuracy of the first approximation) *Let the time step satisfy*

$$\Delta t < \max\left(\frac{\nu^3}{\max_{i=0,1,..,N}\|\nabla\bar{u}(t_i)\|^4}, \frac{C\nu^3}{C_{\nabla\bar{u}}\nu^3 + C_{\bar{u}}\nu^2 + h^{4m}}\right). \tag{2.3.5}$$

Let also $\bar{u} \in L^2(0,T;H^3(\Omega))$ *and* $\bar{u}_{tt} \in L^2(0,T;H^1(\Omega))$. *The error in the first approximation satisfies*

$$\|\bar{u}(t_{n+1}) - w_1^{n+1}\|_A^2 + \nu\Delta t \sum_{i=0}^{n} \|\nabla(\bar{u}(t_{i+1}) - w_1^{i+1})\|^2 + \nu\delta^2\Delta t \sum_{i=0}^{n} \|\zeta(t_{i+1}) - \zeta_1^{i+1}\|^2$$
$$\leq C(\Delta t^2 + \delta^4 + \Delta t \sum_{i=0}^{n}((1+\delta^2 h^{-2}) \inf_{v\in V^h} \|\nabla(\bar{u}(t_i) - v^i)\|^2 + \inf_{q\in Q^h} \|p(t_i) - q^i\|^2)). \tag{2.3.6}$$

Remark 2.3.1 *The restriction of the time step is a blend of two approaches - see inequality* (3.9) *in [7] and inequalities* (4.13), (4.16) *in [18]. The resulting restriction depends upon the regularity of the filtered true solution* $\bar{u}$.

Consider the solution $(w_1^{n+1}, \zeta_1^{n+1}, q_1^{n+1})$ of (2.3.3); denote $e_1^i = \bar{u}(t_i) - w_1^i$ and $g_1^i = \zeta(t_i) - \zeta_1^i$, $i = 0, 1, ..., n+1$. Given below are Theorem 3.3 from [7] and Theorem 3 from [1]; these accuracy results will be needed in the discussion of the correction step approximation.

Theorem 3 (Accuracy of the timestep in the first approximation) *Let the conditions of Theorem 2 be satisfied. Let also* $\bar{u}_t \in L^2(0,T;H^3(\Omega))$ *and* $\bar{u}_{ttt} \in L^2(0,T;H^1(\Omega))$. *Then the following accuracy result holds:*

$$\left\| \frac{e_1^{n+1} - e_1^n}{\Delta t} \right\|_A^2 + \nu \Delta t \sum_{i=0}^{n} \left\| \frac{\nabla(e_1^{i+1} - e_1^i)}{\Delta t} \right\|^2 + \nu \delta^2 \Delta t \sum_{i=0}^{n} \left\| \frac{g_1^{i+1} - g_1^i}{\Delta t} \right\|^2 \tag{2.3.7}$$
$$\leq C(\Delta t^2 + \delta^4 + \Delta t \sum_{i=0}^{n} \inf_{v \in V^h} \left\| \frac{\nabla((\bar{u}(t_{i+1}) - v^{i+1}) - (\bar{u}(t_i) - v^i))}{\Delta t} \right\|^2$$
$$+ \Delta t \sum_{i=0}^{n} \inf_{q \in Q^h} \left\| \frac{(p(t_{i+1}) - q^{i+1}) - (p(t_i) - q^i)}{\Delta t} \right\|^2)$$

Theorem 4 (Accuracy of the Laplacian) *Let the assumptions of Theorem 2 be satisfied. Let also* $\bar{u} \in L^\infty(0,T;L^\infty(\Omega)), \nabla\bar{u} \in L^\infty(0,T;L^\infty(\Omega)), \Delta\bar{u} \in L^2(0,T;H^1(\Omega)) \cap L^\infty(0,T;L^\infty(\Omega))$,
$\nabla\bar{u}_{tt} \in L^2(0,T;H^1(\Omega))$. *Let the time step and the filtering width satisfy* $\Delta t \leq h^{1/2}; \delta \leq h^{1/4}$. *Then the following accuracy result holds for the solution* $(w_1^{n+1}, \zeta_1^{n+1}, q_1^{n+1})$ *of (2.3.3):*

$$\|\nabla(\bar{u}(t_{n+1}) - w_1^{n+1})\|^2 + \delta^2 \|\zeta(t_{n+1}) - \zeta_1^{n+1}\|^2 + \nu \Delta t \sum_{i=0}^{n} \|\zeta(t_{i+1}) - \zeta_1^{i+1}\|^2$$
$$+ \nu \delta^2 \Delta t \sum_{i=0}^{n} \|\nabla(\zeta(t_{n+1}) - \zeta_1^{n+1})\|^2 \leq C(\Delta t^2 + \Delta t^2 \delta^2 +$$
$$\delta^4 + \Delta t \sum_{i=0}^{n} (\inf_{v \in V^h} \|\nabla(\bar{u}(t_i) - v^i)\|^2$$
$$+ \inf_{r \in V^h} \|(\zeta(t_i) - r^i)\|^2 + \min(\delta^{-2}, h^{-2}) \inf_{q \in Q^h} \|p(t_i) - q^i\|^2)) \tag{2.3.8}$$

We are now ready to prove stability and accuracy of the correction step approximation (w_2, ζ_2, q_2).

Theorem 5 (Stability of the second approximation) *Let w_2 satisfy (2.3.4) and let the assumptions of Theorems 1 and 3 be satisfied. Then, for $n = 0, \ldots, N-1$*

$$\begin{aligned} \|w_2^{n+1}\|_A^2 + \nu\Delta t \sum_{i=0}^{n} \|\nabla w_2^{i+1}\|^2 + \delta^2 \nu \Delta t \sum_{i=0}^{n} \|\zeta_2^{i+1}\|^2 \\ \leq \frac{C}{\nu^2} \left(\|w_2^0\|_A^2 + \frac{\Delta t}{\nu} \sum_{i=0}^{n} \left\| \frac{f(t_{i+1}) + f(t_i)}{2} \right\|_{-1}^2 \right) \end{aligned} \tag{2.3.9}$$

PROOF. Take $v^h = w_2^{n+1}$ and $\xi = \zeta_2^{n+1}$ in (2.3.4). Applying Young's inequality along with the definition of $\|f\|_{-1}$ followed by the Cauchy-Schwartz inequality gives:

$$\begin{aligned} \frac{\|w_2^{n+1}\|^2 - \|w_2^n\|^2}{2\Delta t} + \delta^2 \left(\frac{\|\nabla w_2^{n+1}\|^2 - \|\nabla w_2^n\|^2}{2\Delta t} \right) + \nu \|\nabla w_2^{n+1}\|^2 + \nu\delta^2 \|\zeta_2^{n+1}\|^2 \\ \leq 3\epsilon\nu \|\nabla w_2^{n+1}\|^2 + \frac{1}{4\epsilon\nu} \left\| \frac{f(t_{n+1}) + f(t_n)}{2} \right\|_{-1}^2 + \frac{\nu\Delta t^2}{16\epsilon} \left\| \frac{\nabla(w_1^{n+1} - w_1^n)}{\Delta t} \right\|^2 \\ + \frac{\nu\delta^2}{2} \|\zeta_2^{n+1}\|^2 + \frac{\nu\delta^2\Delta t^2}{8} \left\| \frac{\zeta_1^{n+1} - \zeta_1^n}{\Delta t} \right\|^2 + \frac{1}{2} |b^*(w_1^{n+1}, w_1^{n+1}; w_2^{n+1}) - b^*(w_1^n, w_1^n; w_2^{n+1})| \\ + \delta^2 |b^*(\zeta_1^{n+1}, w_1^{n+1}; w_2^{n+1})| + \delta^2 |b^*(w_1^{n+1}, \zeta_1^{n+1}; w_2^{n+1})| + \delta^4 |b^*(\zeta_1^{n+1}, \zeta_1^{n+1}; w_2^{n+1})| \end{aligned} \tag{2.3.10}$$

Note that the pressure terms vanish due to the divergence free condition and the first nonlinear term vanishes by the definition of b^*. We now show that each of the

nonlinear terms is bounded. For the first such term, we make use of equation (2.2.3).

$$|b^*(w_1^{n+1}, w_1^{n+1}, w_2^{n+1}) - b^*(w_1^n, w_1^n, w_2^{n+1})| = \tag{2.3.11}$$
$$\Delta t \left| b^* \left(\frac{w_1^{n+1} - w_1^n}{\Delta t}, w_1^{n+1}; w_2^{n+1} \right) + b^* \left(w_1^n, \frac{w_1^{n+1} - w_1^n}{\Delta t}; w_2^{n+1} \right) \right| \leq$$
$$C\Delta t \left\| \frac{\nabla(w_1^{n+1} - w_1^n)}{\Delta t} \right\| (\|\nabla w_1^{n+1}\| + \|\nabla w_1^n\|)\|w_2^{n+1}\| \leq$$
$$2\epsilon\nu\|w_2^{n+1}\|^2 + \frac{C\Delta t^2}{4\epsilon} \left\| \frac{\nabla(w_1^{n+1} - w_1^n)}{\Delta t} \right\|^2 (\|\nabla w_1^{n+1}\|^2 + \|\nabla w_1^n\|^2)$$

Writing the time difference terms in equations (2.3.11) and (2.3.10) as below, they are bounded using Theorem 3.

$$\left\| \frac{\nabla(w_1^{n+1} - w_1^n)}{\Delta t} \right\|^2 \leq 2 \left\| \frac{\nabla(e_1^{n+1} - e_1^n)}{\Delta t} \right\|^2 + 2 \left\| \frac{\nabla(\bar{u}(t_{n+1}) - \bar{u}(t_n))}{\Delta t} \right\|^2$$

$$\left\| \frac{\zeta_1^{n+1} - \zeta_1^n}{\Delta t} \right\|^2 \leq 2 \left\| \frac{g_1^{n+1} - g_1^n}{\Delta t} \right\|^2 + 2 \left\| \frac{\zeta(t_{n+1}) - \zeta(t_n)}{\Delta t} \right\|^2$$

The next two terms are bounded in a very similar manner, using the results of Theorem 4:

$$\delta^2|b^*(\zeta_1^{n+1}, w_1^{n+1}; w_2^{n+1})| \leq C\delta^2\|\nabla\zeta_1^{n+1}\|\|\nabla w_1^{n+1}\|\|\nabla w_2^{n+1}\|$$
$$\leq \epsilon\nu\|\nabla w_2^{n+1}\|^2 + \frac{C}{\nu^2}(\nu\delta^2\|\nabla\zeta_1^{n+1}\|^2)(\delta^2\|\nabla w_1^{n+1}\|^2)$$

$$\delta^2|b^*(w_1^{n+1}, \zeta_1^{n+1}; w_2^{n+1})|$$
$$\leq \epsilon\nu\|\nabla w_2^{n+1}\|^2 + \frac{C}{\nu^2}(\nu\delta^2\|\nabla\zeta_1^{n+1}\|^2)(\delta^2\|\nabla w_1^{n+1}\|^2)$$

Finally, the last term is bounded by making use of the sharp bound on the nonlinearity and our assumption, $\delta \leq h^{\frac{1}{4}}$ together with the inverse inequality:

$$\delta^4|b^*(\zeta_1^{n+1}, \zeta_1^{n+1}; w_2^{n+1})|$$
$$\leq \delta^4|b^*(\zeta_1^{n+1} - \zeta(t_{n=1}), \zeta_1^{n+1}; w_2^{n+1})| + \delta^4|b^*(\zeta(t_{n+1}), \zeta_1^{n+1}; w_2^{n+1})|$$
$$\leq C\delta^4\|\nabla(\zeta(t_{n+1}) - \zeta_1^{n+1})\|^{\frac{1}{2}}\|\zeta(t_{n+1}) - \zeta_1^{n+1}\|^{\frac{1}{2}}\|\nabla\zeta_1^{n+1}\|\|\nabla w_2^{n+1}\|$$
$$+C\delta^4\|\nabla\zeta(t_{n+1})\|\|\nabla\zeta_1^{n+1}\|\|\nabla w_2^{n+1}\| \leq +2\epsilon\nu\|\nabla w_2^{n+1}\|^2$$
$$+\frac{C\delta^4}{\nu h}(\delta^2\|\zeta(t_{n+1}) - \zeta_1^{n+1}\|^2)(\delta^2\|\nabla w_1^{n+1}\|^2) + \frac{C\delta^6}{\nu^2}\|\nabla\zeta(t_{n+1})\|^2(\nu\delta^2\|\nabla\zeta_1^{n+1}\|^2)$$

Using these bounds on the nonlinear terms leads to

$$\frac{\|w_2^{n+1}\|_A^2 - \|w_2^n\|_A^2}{2\Delta t} + \nu\|\nabla w_2^{n+1}\|^2 + \frac{\nu\delta^2}{2}\|\zeta_2^{n+1}\|^2 \\ \leq 10\epsilon\nu\|\nabla w_2^{n+1}\|^2 + \frac{C}{4\epsilon\nu}\left\|\frac{f(t_{n+1}) + f(t_n)}{2}\right\|_{-1}^2.$$

Choosing $\epsilon = \frac{1}{20}$, multiplying by $2\Delta t$, and summing over all time levels completes the proof.

We now turn our attention to the accuracy of the second approximation. We obtain the equations for the filtered NSE solution by replacing u with $A\bar{u}$ in (1.2.1); then average the filtered NSE over two adjacent time levels, add and subtract the upwind discretization for $A\bar{u}_t$, and rearrange. The filtered true solution $\bar{u}$ satisfies the following equations for all $(v, \xi, \chi) \in (X, X, Q)$.

$$\left(\frac{\bar{u}(t_{n+1})-\bar{u}(t_n)}{\Delta t},v\right)+\delta^2\left(\frac{\nabla\bar{u}(t_{n+1})-\nabla\bar{u}(t_n)}{\Delta t},\nabla v\right)+\nu(\nabla\bar{u}(t_{n+1}),\nabla v)$$

$$+\nu\delta^2(\nabla\zeta(t_{n+1}),\nabla v)+b^*(\bar{u}(t_{n+1}),\bar{u}(t_{n+1});v)-(p(t_{n+1}),\nabla\cdot v)$$

$$=\left(\frac{f(t_{n+1})+f(t_n)}{2},v\right)$$

$$+\frac{\Delta t}{2}\nu\left(\frac{\nabla\bar{u}(t_{n+1})-\nabla\bar{u}(t_n)}{\Delta t},\nabla v\right)+\frac{\Delta t}{2}\nu\delta^2\left(\frac{\nabla\zeta(t_{n+1})-\nabla\zeta(t_n)}{\Delta t},\nabla v\right)$$

$$+\frac{1}{2}b^*(\bar{u}(t_{n+1}),\bar{u}(t_{n+1});v)-\frac{1}{2}b^*(\bar{u}(t_n),\bar{u}(t_n);v)-\frac{\Delta t}{2}\left(\frac{p(t_{n+1})-p(t_n)}{\Delta t},\nabla\cdot v\right)$$

$$-\delta^2b^*(\zeta(t_{n+1}),\bar{u}(t_{n+1});v)-\delta^2b^*(\bar{u}(t_{n+1}),\zeta(t_{n+1});v)-\delta^4b^*(\zeta(t_{n+1}),\zeta(t_{n+1});v)$$

$$+\frac{\delta^2}{2}(b^*(\zeta(t_{n+1}),\bar{u}(t_{n+1});v)-b^*(\zeta(t_n),\bar{u}(t_n);v))$$

$$+\frac{\delta^2}{2}(b^*(\bar{u}(t_{n+1}),\zeta(t_{n+1});v)-b^*(\bar{u}(t_n),\zeta(t_n);v))$$

$$+\frac{\delta^4}{2}(b^*(\zeta(t_{n+1}),\zeta(t_{n+1});v)-b^*(\zeta(t_n),\zeta(t_n);v))$$

$$+\left(A\left(\frac{\bar{u}_t(t_{n+1})+\bar{u}_t(t_n)}{2}-\frac{\bar{u}(t_{n+1})-\bar{u}(t_n)}{\Delta t}\right),v\right),$$

$$(\nabla\bar{u}(t_{n+1}),\nabla\xi)=(\zeta(t_{n+1}),\xi),$$

$$(\nabla\cdot\bar{u}(t_{n+1}),\chi)$$

(2.3.12)

Theorem 6 (Accuracy of the Second Approximation) *Let the assumptions of Theorems 2-4 be satisfied. Then there exists a constant C such that the following accuracy bound holds for the solution (w_2,ζ_2,q_2) of (2.3.4):*

$$\|\bar{u}(t_{n+1}) - w_2^{n+1}\|_A^2 + \nu\Delta t \sum_{i+0}^{n} \|\nabla(\bar{u}(t_{n+1}) - w_2^{n+1})\|^2$$

$$+\nu\delta^2\Delta t \sum_{i=0}^{n} \|\zeta(t_{n+1}) - \zeta_2^{n+1}\|^2 \leq C(\Delta t^4 + \Delta t^2\delta^4 + \delta^8$$

$$\Delta t \sum_{i=0}^{n} ((1+\delta^2 h^{-2}) \inf_{v\in X^h} \|\nabla(\bar{u}(t_i) - v^i)\|^2 + (1+\delta^4 h^{-2}) \inf_{v\in X^h} \|\bar{u}_t(t_i) - v^i\|^2$$

$$+ \inf_{q\in Q^h} \|p(t_i) - q^i\|^2 + \inf_{r\in X^h} \|(\zeta(t_i) - r^i)\|^2))$$

$$+\Delta t^2(\nu\Delta t \sum_{i=0}^{n} \inf_{v\in V^h} \left\| \frac{\nabla((\bar{u}(t_{i+1}) - v^{i+1}) - (\bar{u}(t_i) - v^i))}{\Delta t} \right\|^2$$

$$+\Delta t \sum_{i=0}^{n} \inf_{q\in Q^h} \left\| \frac{(p(t_{i+1}) - q^{i+1}) - (p(t_i) - q^i)}{\Delta t} \right\|^2$$

$$+\nu\delta^4\Delta t \sum_{i=0}^{n} \inf_{r\in V^h} \left\| \frac{(\zeta(t_{i+1}) - r^{i+1}) - \zeta(t_i) - r^i)}{\Delta t} \right\|^2))$$

PROOF: Subtract (2.3.4) from (2.3.12) and decompose the error such that $e_2^{n+1} = \bar{u}(t_{n+1}) - w_2^{n+1} = \phi^{n+1} - \eta^{n+1}$ and $\zeta(t_{n+1}) - \zeta_2^{n+1} = \psi^{n+1} - \mu^{n+1}$, where $\phi^{n+1} \in V^h$ and $\psi^{n+1} \in V^h$. Choosing $v^h = \phi^{n+1}$, $\xi^h = \psi^{n+1}$, and applying the Cauchy-Schwartz and Young inequalities gives

$$\frac{\|\phi^{n+1}\|^2-\|\phi^n\|^2}{2\Delta t}+\delta^2\frac{\|\nabla\phi^{n+1}\|^2-\|\nabla\phi^n\|^2}{2\Delta t}+\nu\|\nabla\phi^{n+1}\|^2+\nu\delta^2\|\psi^{n+1}\|^2\leq$$
$$\epsilon\nu\|\nabla\phi^{n+1}\|^2+\frac{1}{4\epsilon\nu}\left\|\frac{\eta^{n+1}-\eta^n}{\Delta t}\right\|_{-1}^2+\epsilon\nu\|\nabla\phi^{n+1}\|^2+\frac{\delta^4}{4\epsilon\nu}\left\|\frac{\nabla(\eta^{n+1}-\eta^n)}{\Delta t}\right\|^2$$
$$+2\epsilon_1\nu\delta^2\|\psi^{n+1}\|^2+\frac{\nu\delta^2}{4\epsilon_1}\|\Delta\eta^{n+1}\|^2$$
$$+\frac{\nu\delta^2}{4\epsilon_1}\|\mu^{n+1}\|^2+\epsilon\nu\|\nabla\phi^{n+1}\|^2+\frac{\delta^4}{4\nu\epsilon}\|\nabla\mu^{n+1}\|^2$$
$$+\epsilon\nu\|\nabla\phi^{n+1}\|^2+\frac{3}{4\epsilon\nu}\|p(t_{n+1})-q_2^{n+1}\|^2$$
$$+\epsilon\nu\|\nabla\phi^{n+1}\|^2+\frac{\nu\Delta t^2}{16\epsilon}\left\|\frac{\nabla(e_1^{n+1}-e_1^n)}{\Delta t}\right\|^2$$
$$+\epsilon\nu\|\nabla\phi^{n+1}\|^2+\frac{\nu\delta^4\Delta t^2}{16\epsilon}\left\|\frac{\nabla(g_1^{n+1}-g_1^n)}{\Delta t}\right\|^2$$
$$+\epsilon\nu\|\nabla\phi^{n+1}\|^2+\frac{3\Delta t^2}{16\epsilon\nu}\left\|\frac{(p(t_{n+1})-q_2^{n+1})-(p(t_n)-q_2^n)}{\Delta t}\right\|^2$$
$$+|b^*(\bar{u}(t_{n+1}),\bar{u}(t_{n+1});\phi^{n+1})-b^*(w_2^{n+1},w_2^{n+1};\phi^{n+1})|$$
$$+\delta^2|b^*(\bar{u}(t_{n+1}),\zeta(t_{n+1});\phi^{n+1})-b^*(w_1^{n+1},\zeta_1^{n+1};\phi^{n+1})|$$
$$+\delta^2|b^*(\zeta(t_{n+1}),\bar{u}(t_{n+1});\phi^{n+1})-b^*(\zeta_1^{n+1},w_1^{n+1};\phi^{n+1})|$$
$$+\delta^4|b^*(\zeta(t_{n+1}),\zeta(t_{n+1});\phi^{n+1})-b^*(\zeta_1^{n+1},\zeta_1^{n+1};\phi^{n+1})|$$
$$+\frac{\delta^2}{2}|b^*(\bar{u}(t_{n+1}),\zeta(t_{n+1});v^h)-b^*(\bar{u}(t_n),\zeta(t_n);v^h)|$$
$$+\frac{\delta^2}{2}|b^*(\zeta(t_{n+1}),\bar{u}(t_{n+1});v^h)-b^*(\zeta(t_n),\bar{u}(t_n);v^h))$$
$$+\frac{\delta^4}{2}|b^*(\zeta(t_{n+1}),\zeta(t_{n+1});v^h)-b^*(\zeta(t_n),\zeta(t_n);v^h)|$$
$$+\left|\left(A\left(\frac{\bar{u}_t(t_{n+1})+\bar{u}_t(t_n)}{2}-\frac{\bar{u}(t_{n+1})-\bar{u}(t_n)}{\Delta t}\right),v^h\right)\right| \quad (2.3.13)$$

We will now bound each of the nonlinear terms in turn. Considering the first nonlinear term, we add and subtract $b^*(w_2^{n+1}, \bar{u}(t_{n+1}); \phi^{n+1})$ to get

$$\begin{aligned}
|b^*(\bar{u}(t_{n+1}), \bar{u}(t_{n+1}); \phi^{n+1}) - b^*(w_2^{n+1}, w_2^{n+1}; \phi^{n+1})| \leq \\
|b^*(\phi^{n+1} - \eta^{n+1}, \bar{u}(t_{n+1}); \phi^{n+1})| + |b^*(w_2^{n+1}, \phi^{n+1} - \eta^{n+1}; \phi^{n+1})| \leq \\
|b^*(\phi^{n+1}, \bar{u}(t_{n+1}); \phi^{n+1})| + |b^*(\eta^{n+1}, \bar{u}(t_{n+1}); \phi^{n+1})| + |b^*(w_2^{n+1}, \eta^{n+1}; \phi^{n+1})| \leq \\
|b^*(\phi^{n+1}, \bar{u}(t_{n+1}); \phi^{n+1})| + |b^*(\eta^{n+1}, \bar{u}(t_{n+1}); \phi^{n+1})| \\
+|b^*(\bar{u}(t_{n+1}), \eta^{n+1}; \phi^{n+1})| + |b^*(\phi^{n+1}, \eta^{n+1}; \phi^{n+1})| + |b^*(\eta^{n+1}, \eta^{n+1}; \phi^{n+1})|
\end{aligned}$$

And these five terms are bounded as follows

$$\begin{aligned}
|b^*(\phi^{n+1}, \bar{u}(t_{n+1}); \phi^{n+1})| &\leq \epsilon\nu\|\nabla\phi^{n+1}\|^2 + C\nu^{-3}\|\nabla\bar{u}(t_{n+1})\|^4\|\phi^{n+1}\|^2 \\
|b^*(\eta^{n+1}, \bar{u}(t_{n+1}); \phi^{n+1})| &\leq \epsilon\nu\|\nabla\phi^{n+1}\|^2 + C \cdot C_{\nabla\bar{u}}^2\nu^{-1}\|\nabla\eta^{n+1}\|^2 \\
|b^*(\bar{u}(t_{n+1}), \eta^{n+1}; \phi^{n+1})| &\leq \epsilon\nu\|\nabla\phi^{n+1}\|^2 + C \cdot C_{\nabla\bar{u}}^2\nu^{-1}\|\nabla\eta^{n+1}\|^2 \\
|b^*(\phi^{n+1}, \eta^{n+1}; \phi^{n+1})| &\leq \epsilon\nu\|\nabla\phi^{n+1}\|^2 + C\nu^{-3}\|\nabla\eta^{n+1}\|^4\|\phi^{n+1}\|^2 \\
|b^*(\eta^{n+1}, \eta^{n+1}; \phi^{n+1})| &\leq \epsilon\nu\|\nabla\phi^{n+1}\|^2 + C\nu^{-1}\|\nabla\eta^{n+1}\|^4
\end{aligned}$$

The first two $O(\delta^2)$ terms and the first $O(\delta^4)$ term in equation 2.3.13 are bounded as follows.

$$\begin{aligned}
\delta^2|b^*(\bar{u}(t_{n+1}),\zeta(t_{n+1});\phi^{n+1}) - b^*(w_1^{n+1},\zeta_1^{n+1};\phi^{n+1})| \leq \\
\delta^2|b^*(\bar{u}(t_{n+1}),\zeta(t_{n+1});\phi^{n+1}) - b^*(\bar{u}(t_{n+1}),\zeta_1^{n+1};\phi^{n+1})| \\
+\delta^2|b^*(\bar{u}(t_{n+1}),\zeta_1^{n+1};\phi^{n+1}) - b^*(w_1^{n+1},\zeta_1^{n+1};\phi^{n+1})| \leq \\
C\cdot C_{\bar{u}}\delta^2\|\zeta(t_{n+1}) - \zeta_1^{n+1}\|\|\nabla\phi^{n+1}\| \\
+\delta^2 C\|\nabla(\bar{u} - w_1^{n+1})\|\|\nabla(\zeta(t_{n+1}) - \zeta_1^{n+1})\|\|\nabla\phi^{n+1}\| \\
+C\cdot C_{\nabla\zeta}\delta^2\|\nabla(\bar{u} - w_1^{n+1})\|\|\nabla\phi^{n+1}\| \leq \\
3\nu\epsilon\|\nabla\phi^{n+1}\|^2 + C\cdot C_{\bar{u}}^2\delta^4\nu^{-2}(\nu\|\zeta(t_{n+1}) - \zeta_1^{n+1}\|^2) + C\cdot C_{\nabla\zeta}^2\delta^4\|\nabla(\bar{u} - w_1^{n+1})\|^2 \\
+C\delta^2\nu^{-2}(\nu\delta^2\|\nabla(\zeta(t_{n+1}) - \zeta_1^{n+1})\|^2)(\|\nabla(\bar{u}(t_{n+1}) - w_1^{n+1})\|^2)
\end{aligned}$$

$$\begin{aligned}
\delta^2|b^*(\zeta(t_{n+1}),\bar{u}(t_{n+1});\phi^{n+1}) - b^*(\zeta_1^{n+1},w_1^{n+1};\phi^{n+1})| \leq \\
3\nu\epsilon\|\nabla\phi^{n+1}\|^2 + C\cdot C_{\nabla\bar{u}}^2\delta^4\nu^{-2}(\nu\|\zeta(t_{n+1}) - \zeta_1^{n+1}\|^2) + C\cdot C_{\zeta}^2\delta^4\|\nabla(\bar{u} - w_1^{n+1})\|^2 \\
+C\delta^2\nu^{-2}(\nu\delta^2\|\nabla(\zeta(t_{n+1}) - \zeta_1^{n+1})\|^2)(\|\nabla(\bar{u}(t_{n+1}) - w_1^{n+1})\|^2)
\end{aligned}$$

$$\begin{aligned}
\delta^4|b^*(\zeta(t_{n+1}),\zeta(t_{n+1});\phi^{n+1}) - b^*(\zeta_1^{n+1},\zeta_1^{n+1};\phi^{n+1})| \leq \\
2\nu\epsilon\|\nabla\phi^{n+1}\|^2 + C\cdot C_{\zeta}^2\delta^6\nu^{-1}(\delta^2\|\zeta(t_{n+1}) - \zeta_1^{n+1}\|^2) \\
+C\delta^4 h^{-1}\nu^{-2}(\nu\delta^2\|\nabla(\zeta(t_{n+1}) - \zeta_1^{n+1})\|^2)(\delta^2\|\zeta(t_{n+1}) - \zeta_1^{n+1})\|^2)
\end{aligned}$$

The remaining terms of 2.3.13 are bounded as below. The first trilinear term is given. The last two are very similar. The last term includes the difference of two $O(\Delta t^2)$ approximations for $\bar{u}(t_{n+\frac{1}{2}})$.

$$\delta^2|b^*(\bar{u}(t_{n+1}),\zeta(t_{n+1});\phi^{n+1}) - b^*(\bar{u}(t_n),\zeta(t_n);\phi^{n+1})| \leq$$

$$\delta^2|b^*(\bar{u}(t_{n+1}),\zeta(t_{n+1})-\zeta(t_n);\phi^{n+1})| + \delta^2|b^*(\bar{u}(t_{n+1})-\bar{u}(t_n),\zeta(t_{n+1});\phi^{n+1})| \leq$$

$$+\epsilon\nu\|\nabla\phi^{n+1}\|^2 + C\delta^4\Delta t^2\|\nabla\bar{u}(t_{n+1})\|^2\left\|\frac{\nabla(\zeta(t_{n+1})-\zeta(t_n))}{\Delta t}\right\|^2$$

$$+\epsilon\nu\|\nabla\phi^{n+1}\|^2 + C\delta^4\Delta t^2\|\nabla\zeta(t_{n+1})\|^2\left\|\frac{\nabla(\bar{u}(t_{n+1})-\bar{u}(t_n))}{\Delta t}\right\|^2$$

$$\left|\left(A\left(\frac{\bar{u}_t(t_{n+1})+\bar{u}_t(t_n)}{2} - \frac{\bar{u}(t_{n+1})-\bar{u}(t_n)}{\Delta t}\right),\phi^{n+1}\right)\right| \leq$$

$$O(\Delta t^4 + \Delta t^4\delta^4) + 2\epsilon\nu\|\nabla\phi^{n+1}\|^2$$

Now choosing $\epsilon = \frac{1}{58}$, $\epsilon_1 = \frac{1}{4}$, multiplying by $2\Delta t$, summing over all time levels, and applying Lemma 3 completes the proof.

2.4 Numerical Tests

In order to numerically investigate the proposed model, three benchmark problems will be considered in this Section. We will start by verifying the claimed convergence rates, when the model is applied to a problem with a known true solution. Next, we apply the model to a flow past the full step, and show that the correction step approximation w_2 captures the qualitative features of the true solution in a much more accurate way, than does the defect step approximation w_1. Finally, the model will be tested on a benchmark problem, that is quantitative, rather than qualitative: the computation of drag and lift coefficients in the flow past a cylinder. All problems in this Section are two-dimensional, and the computations were performed using the FreeFEM++ software, [19].

2.4.1 Convergence Rates

In this subsection, we apply the ADC model (2.3.3) − (2.3.4) to a problem with known true solution. The errors and the convergence rates will be computed for the values of the viscosity coefficient, typically associated with transitional flows, $\nu = 10^{-3}$, and fully developed turbulence, $\nu = 10^{-5}$. The space-time domain is $\{0.5 \leq x \leq 1, 0.5 \leq y \leq 1, 0.25 \leq t \leq 0.75\}$, and the solution of the test problem is

given by

$$u_1 = \tfrac{3}{4} + \tfrac{1}{4}\ \cos(2\pi(\mathrm{x} - \mathrm{t}))\sin(2\pi(y-t))e^{(-8\pi^2 t\nu)},$$

$$u_2 = \tfrac{3}{4} - \tfrac{1}{4}\ \sin(2\pi(\mathrm{x} - \mathrm{t}))\cos(2\pi(y-t))e^{(-8\pi^2 t\nu)},$$

$$p = -\tfrac{1}{64}\ \cos(4\pi(\mathrm{x} - \mathrm{t}))\cos(4\pi(y-t))e^{(-16\pi^2 t\nu)}.$$

First we compute the errors and convergence rates for the defect step approximation w_1 and the correction step solution w_2 on a uniform mesh, as the mesh diameter, time step and filtering width are being refined, $\delta = h = \Delta t$. In this case, the theory predicts the first order accuracy, $O(h^2 + \delta^2 + \Delta t) = O(h)$, for the defect step approximation. The correction step should produce a second order accurate approximation, $O(h^2 + \delta^4 + \Delta t^2) = O(h^2)$. The results, given in Tables 2.1 - 2.2, demonstrate the claimed convergence rates (N represents the number of points on one side of the boundary, $h = \frac{1}{2N}$).

The Approximate Deconvolution Model (ADM) - and, subsequently, the corresponding LES-C model ADC, discussed herein - aims to approximate the filtered velocity and non-filtered pressure $(\bar{u}, p)$. Thus, in order to verify the claimed convergence rates, we first calculate the filtered solution on the given mesh with given filtering

width δ, satisfying

$$\bar{u} - \delta^2 \Delta \bar{u} = u \text{ in } \Omega, \qquad \bar{u} = u \text{ on } \partial\Omega,$$

and then compare it against the model solutions w_1, w_2. In the calculation of $\bar{u}$ an extra error is committed, as it is not possible to derive the correct boundary conditions for $\bar{u}$ on $\partial\Omega$, based on the values of $u \in \Omega$.

Table 2.1
Errors in (2.3.3) and (2.3.4), $\nu = 10^{-3}$, $\delta = h = \Delta t$

N	$\|\|\bar{u} - \omega_1\|\|_{L^2(L^2)}$	$\|\|\bar{u} - \omega_2\|\|_{L^2(L^2)}$	$\|\|\bar{u} - \omega_1\|\|_{L^2(H^1)}$	$\|\|\bar{u} - \omega_2\|\|_{L^2(H^1)}$
16	0.00710468	0.00723822	0.173303	0.350676
32	0.00423811	0.00269028	0.140095	0.238938
64	0.00227292	0.000675002	0.0914498	0.0972327

Table 2.2
Convergence rates for errors in Table 2.1

$\omega_1 \in L^2(L^2)$	$\omega_2 \in L^2(L^2)$	$\omega_1 \in L^2(H^1)$	$\omega_2 \in L^2(H^1)$
0.75	1.43	0.31	0.55
0.90	1.99	0.62	1.30

The defect correction methods are known for having only asymptotic convergence properties - and it might seem from these tables, that more mesh refinements are needed to capture the correct convergence rates in the energy norm. However, as the next results demonstrate, it suffices to reduce only the time step and the filtering width, in order to see the correct convergence rates on a fixed mesh.

We create a quasi-uniform mesh with $N_1 = 64$ points on the left and bottom walls of the domain, and $N_2 = 80$ mesh nodes on the right and top boundaries: the mesh diameter is $h = \frac{1}{2N_1} = \frac{1}{128}$. With this mesh being fixed, we refine the time step and filtering width. The errors and convergence rates are given in Tables 2.3 - 2.4. Note that the mesh is quasi-uniform, which results in the difference between the values in the first row of Table 2.3 and those in the last row of Table 2.1.

Table 2.3
Errors in (2.3.3) and (2.3.4), $\nu = 10^{-3}$, spatial mesh is fixed at $h = \frac{1}{128}$, while the time step and filtering width are refined.

N	$\|\|\bar{u} - \omega_1\|\|_{L^2(L^2)}$	$\|\|\bar{u} - \omega_2\|\|_{L^2(L^2)}$	$\|\|\bar{u} - \omega_1\|\|_{L^2(H^1)}$	$\|\|\bar{u} - \omega_2\|\|_{L^2(H^1)}$
h	0.00227971	0.000657181	0.0900065	0.0940873
h/2	0.00117971	0.000147313	0.0544724	0.0311926
h/4	0.000600011	2.97E-05	0.0311129	0.00846719
h/8	0.000302609	5.58E-06	0.0169704	0.00188764

Table 2.4
Convergence rates for errors in Table 2.3

$\omega_1 \in L^2(L^2)$	$\omega_2 \in L^2(L^2)$	$\omega_1 \in L^2(H^1)$	$\omega_2 \in L^2(H^1)$
0.95	2.16	0.72	1.59
0.98	2.31	0.81	1.88
0.99	2.41	0.87	2.17

Several conclusions can be drawn from Tables 2.3 - 2.4. First, comparing the results in Tables 2.1-2.2 to those in Tables 2.3 - 2.4, we deduce that the component of the overall error, stemming from the finite element approximation, is small compared to the modeling and time discretization error components. Secondly, as the filtering width and the time step are being refined, we clearly see the advantage of the correction

step approximation over the defect step - both in the reduced absolute values of the errors, and in the improved convergence rates. Finally, as the convergence rates of $||\bar{u} - \omega_2||_{L^2(0,T;L^2(\Omega))}$ and $||\bar{u} - \omega_2||_{L^2(0,T;H^1(\Omega))}$ increase past the value 2, we conclude that the claimed second order convergence with respect to the time step has been verified. The next example in this subsection will show that, as we keep reducing the time step and the filtering width, these rates increase even further - suggesting that the rate of convergence with respect to the filtering width is at least 3, even in the case of a much higher Reynolds number. This does not fully verify the claimed fourth order accuracy with respect to the filtering width, and further refinements of the time step and, possibly, spatial mesh, might be needed to verify the fourth order accuracy.

Next we will further reduce the viscosity coefficient, letting $\nu = 10^{-5}$. While the true solution is still smooth, we expect this to be a more challenging test for our model. As in the previous case, we fix the mesh with $N_1 = 64$, $N_2 = 80$, $h = \frac{1}{128}$, and refine the filtering width and the time step simultaneously, always keeping $\delta = \Delta t$. The results, shown in Tables 2.5 - 2.6, again show the clear advantage of the correction step solution over the defect step solution; the convergence rates are as predicted by the theory, although a few extra refinements of the filtering width and time step (on the same spatial mesh) might be needed to achieve these rates. The convergence rates of the defect step approximation decrease as the time step and the filtering width become too small - indicating that the finite element error becomes a bigger part of

the overall error. However, the convergence rates of the correction step solution are still approaching the values claimed by the theory - and, more importantly, the error in approximating the true solution by the correction step solution w_2 becomes seven times smaller than the error from the defect step approximation w_1.

Table 2.5
Errors in (2.3.3) and (2.3.4), $\nu = 10^{-5}$, spatial mesh is fixed at $h = \frac{1}{128}$, while the time step and filtering width are refined.

$\delta = \Delta t$	$\|\|\bar{u} - \omega_1\|\|_{L^2(L^2)}$	$\|\|\bar{u} - \omega_2\|\|_{L^2(L^2)}$	$\|\|\bar{u} - \omega_1\|\|_{L^2(H^1)}$	$\|\|\bar{u} - \omega_2\|\|_{L^2(H^1)}$
h	0.00245446	0.00981675	0.223553	5.73065
h/2	0.00127319	0.00290769	0.170311	2.70714
h/4	0.00066767	0.00107661	0.16385	0.959415
h/8	0.000381481	0.000369831	0.163266	0.291716
h/16	0.00022466	8.21E-05	0.119295	0.0609031
h/32	0.000121875	1.32E-05	0.0683414	0.00941398

Table 2.6
Convergence rates for errors in Table 2.5

$\omega_1 \in L^2(L^2)$	$\omega_2 \in L^2(L^2)$	$\omega_1 \in L^2(H^1)$	$\omega_2 \in L^2(H^1)$
0.95	1.76	0.39	1.08
0.93	1.43	0.06	1.50
0.81	1.54	0.01	1.72
0.76	2.17	0.45	2.26
0.88	2.64	0.80	2.69

2.4.2 Flow Past the Full Step

For the next step of validating the model (2.3.3)-(2.3.4), we consider the benchmark problem of flow past the forward-backward facing step. This model has been commonly used in numerical tests of turbulence models and regularization techniques for the NSE - see, e.g., [1, 20, 21, 22, 23]. It is known that for $500 \leq Re \leq 700$ a recirculation region is clearly seen behind the step, where vortices are formed; with time, they shed, deform and travel with the flow.

Following the setting of, e.g., [22], we consider the domain $[0, 40] \times [0, 10]$ with the step of unit height at $5 \leq x \leq 6$. For both model solutions w_1 and w_2 we impose the parabolic inflow and outflow boundary conditions $u_i = y(10 - y)/25, v_i = 0$, where $w_i = (u_i, v_i)^T$, $i = 1, 2$. No-slip boundary conditions are imposed on the rest of the boundary. The Reynolds number is fixed at $Re = 600$, and the time step is $\Delta t = 0.005$.

We present the results, obtained at a very coarse mesh with only $6,010$ degrees of freedom (dofs). These are compared against the reference solution, obtained by solving the NSE system with Crank-Nicolson time discretization (CN) at a very fine mesh of $86,125$ dofs. As another point of comparison, we consider the results of [1], where a mesh with $8,897$ dofs was used in combination with the ADC model and

Crank-Nicolson time discretization. In all the results, presented in this subsection, the filtering width was fixed at $\delta = 0.125$. The results are presented in Figure 2.1 below. When compared to the CN-NSE and CN-ADC solutions, given in Figure 2.2, we see that the correction step solution w_2 of (2.3.4) produces the flow that is qualitatively much closer to the reference solution, than the defect step solution w_1 of (2.3.3). Even on such a coarse mesh, the correction step solution is able to correctly predict the process of vortices forming, shedding and traveling.

The CN-NSE solution plays the role of the "true" solution here, as it is computed without any modeling ($\delta = 0$), on a much finer spatial mesh, and it has the verified second order convergence (as opposed to the asymptotic convergence of the ADC solution to second order accuracy) w.r.t. the time step. Thus, comparing the ADC solution against the CN-NSE solution, we show that we can capture the qualitative features of the DNS (direct numerical simulation) solution, while using a substantially coarser mesh.

The plot in Figure 2.2(b) shows the CN-ADC solution, where the ADC has already been implemented in space (with $\delta = 1/8$), but the Crank-Nicolson method was used for time discretization. This could be viewed as a solution "half way" between the proposed full ADC (Figure 2.1(h)) and the "true" DNS solution in Figure 2.2(a). When viewing the development from Figure 2.2(b) to Figure 2.1(h) to Figure 2.2(a), one can see that the qualitative behavior of the solution is captured well by the

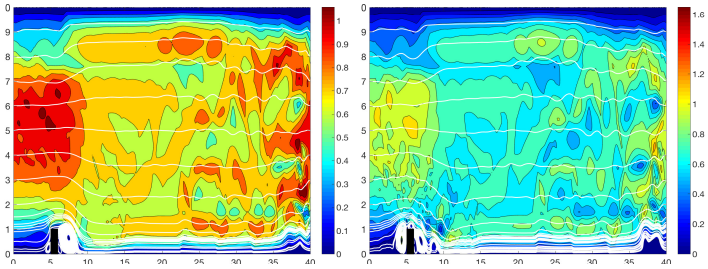

(a) Defect Step Solution at t=10

(b) Correction Step Solution at t=10

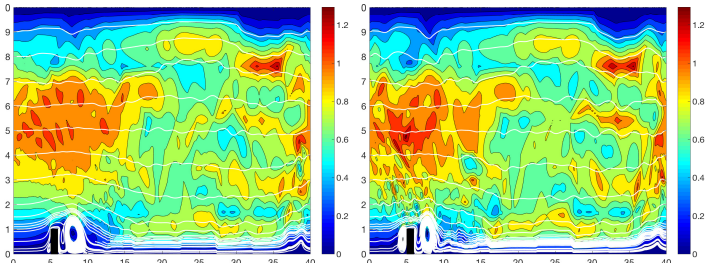

(c) Defect Step Solution at t=20

(d) Correction Step Solution at t=20

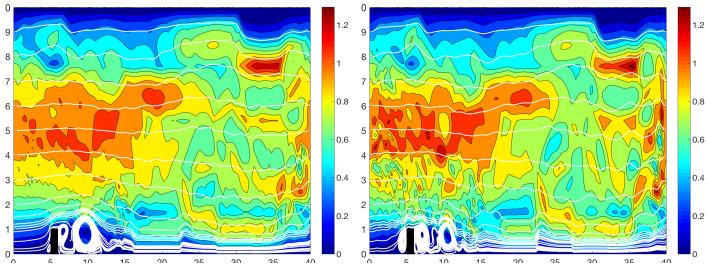

(e) Defect Step Solution at t=30

(f) Correction Step Solution at t=30

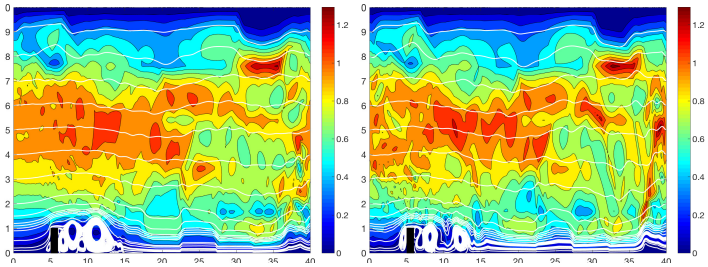

(g) Defect Step Solution at t=40

(h) Correction Step Solution at t=40

Figure 2.1: Time evolution of the flow, captured by the Defect Step solution (left) vs. the Correction Step solution (right column).

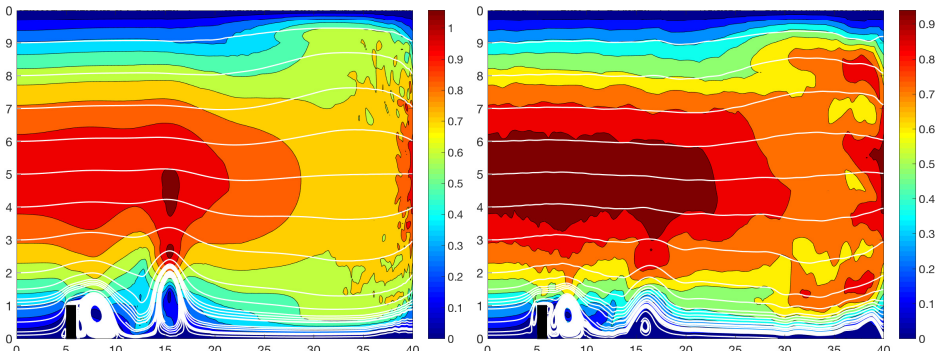

(a) CN-NSE solution at t=40; 86,125 dofs

(b) Correction Step Solution at t=40; 8,897 dofs

Figure 2.2: CN-NSE solution at a very fine mesh (left) and the CN-ADC solution of [1] (right) at $T = 40$.

proposed method. One can also use Figure 2.1(h) to attribute the delay in the vortex motion of Figure 2.2(b) to the deferred correction - the correction of the time discretization error. Notice also, that the proposed model used Backward Euler as the time discretization method for the defect step; this can be replaced with Crank-Nicolson or any other method with sufficient stability properties, and the deferred correction would then improve the quality of the solution even beyond that of the Crank-Nicolson approximation.

2.4.3 Flow Past 3D Step

In this subsection we consider the 3D analogue of the previous test problem: flow past a step. The region is given by $\Omega = [0, 40] \times [0, 10] \times [0, 10]$, with the step at $5 \leq x \leq 6, 0 \leq z \leq 1$. Parabolic inflow is prescribed at the left wall $x = 0$, and it is

given by $u_1 = z*(10-z)/25$. The computations are performed at a very coarse mesh with only $33,204$ dofs, with the Reynolds number $Re = 600$. The reference solution is obtained by solving the NSE with Crank-Nicolson time discretization (CN-NSE), and with the time step $\Delta t = 1/16$. The time step for the ADC model is chosen to be $\Delta t = 1/8$, so that the CN-NSE solution could be viewed as a "true" solution. The streamlines, plotted in Figure 2.3, clearly capture the wave front traveling near the plane $x = 17$ in both the CN-NSE solution and the ADC Correction step solution. To the contrary, this front is not adequately predicted by the solution of the Defect step of the ADC, which is the ADM with Backward Euler time discretization.

Another way of viewing these solutions is presented in Figure 2.4, where the solutions are projected onto the plane $y = 5$. Again, the waves travelling at or near the plane $x = 17$ are visible in the CN-NSE solution and the ADC-Correction step solution, but they are not captured by the ADC-Defect step solution.

2.4.4 Drag and Lift Coefficients

Referring now the problem outlined in chapter 1, the following data will be collected from this experiment, and compared against the results in the literature: maximal values of the drag and lift coefficients, the times when these values were attained, and the difference of pressure before and after the obstacle at the final time, $\Delta p(8)$, where

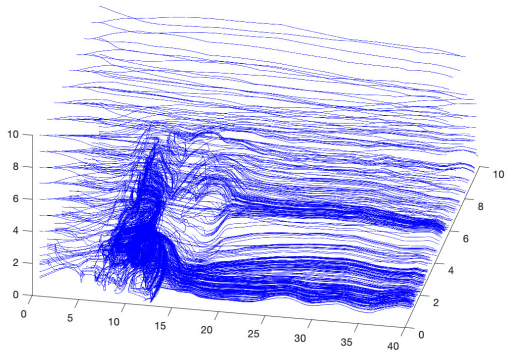

(a) CN-NSE solution at T=40; 33,204 dofs; $\Delta t = 1/16$

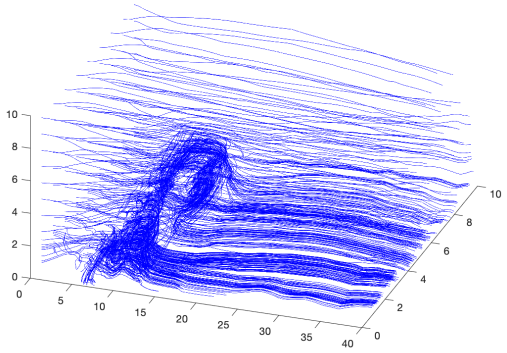

(b) Defect Step Solution at T=40; 33,204 dofs; $\Delta t = 1/8$

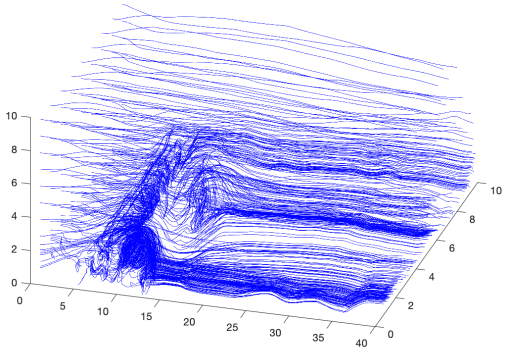

(c) Correction Step Solution at T=40; 33,204 dofs; $\Delta t = 1/8$

Figure 2.3: Solutions at a coarse mesh: (a) reference CN-NSE solution at $\Delta t = 1/16$; (b) ADC Defect Step Solution at $\Delta t = 1/8$; (c) ADC Correction Step Solution at $\Delta t = 1/8$.

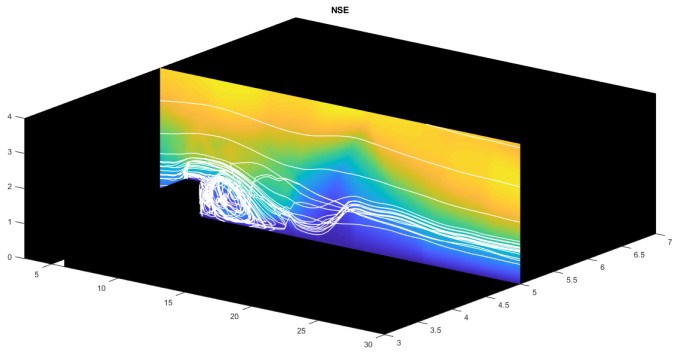

(a) CN-NSE solution at $y = 5$

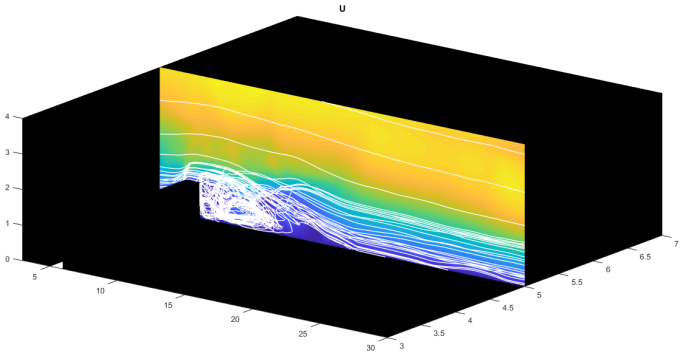

(b) Defect Step Solution at $y = 5$

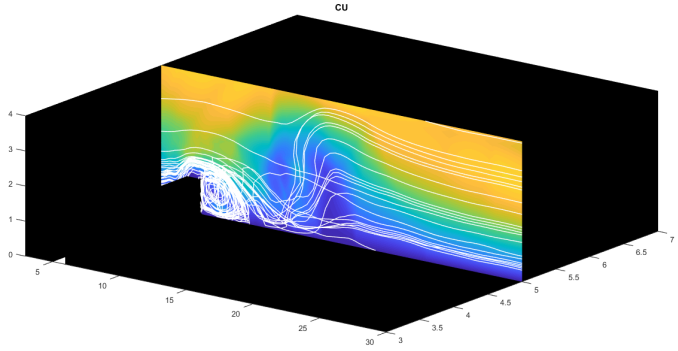

(c) Correction Step Solution at at $y = 5$

Figure 2.4: Solutions from Figure 2.3, projected onto the midplane $y = 5$.

$\Delta p(t) = p(t; 0.15, 0.2) - p(t; 0.25, 0.2)$. We aim to demonstrate the clear advantage of the correction step solution w_2 over the defect step solution w_1. This test is not very well suited for the Approximate Deconvolution-based models, because these models, including the ADC model of this chapter, aim to approximate the filtered solution $\bar{u}$ - not the exact velocity field u. Nevertheless, in the computations below we will use the exact deconvolution of the model's solutions, Aw_1 and Aw_2, as our approximation of the exact velocity field u. Throughout this subsection the mesh will be fixed, with the number of degrees of freedom being $23,392$ for velocity and $3,004$ for pressure (compared to $25,408$ and $3,248$ in [2], level 2). The filtering width is also fixed, with $\delta = \frac{1}{8}h$. The only parameters that is being modified in this test problem is the time step; thus, the performance of the model solutions w_1 and w_2 could be attributed to the model's treatment of the time discretization.

As the time step is being refined, we check the performance of the defect step and correction step solutions: the drag and lift coefficients, as well as pressure difference, must approach the reference intervals given in chapter 1 for these values.

In Tables 3.1-2.9 below we report the error, computed as the shortest distance from the computed quantity of interest to the corresponding reference interval. Upper script values $1, 2$ correspond to the defect and correction steps, respectively.

We notice from the tables above that the maximal drag coefficient is the least sensitive among the quantities of interest (the authors of [2] arrived at the same conclusion),

Table 2.7
Maximal Drag Coefficients

Δt	$c^1_{d,max}$	Error^1	$t(c^1_{d,max})$	$c^2_{d,max}$	Error^2	$t(c^2_{d,max})$
0.04	2.92099	0.00901	3.92	2.97026	0.00026	3.92
0.02	2.92046	0.00954	3.92	2.97028	0.00028	3.94
0.01	2.92022	0.00978	3.93	2.97033	0.00033	3.93
0.005	2.92108	0.00892	3.93	2.97135	0.00135	3.93
0.0025	2.92107	0.00893	3.92	2.97156	0.00156	3.92
0.00125	2.92113	0.00887	3.92875	2.9717	0.0017	3.93375
0.000625	2.92119	0.00881	3.92875	2.97178	0.00178	3.93375

Table 2.8
Maximal Lift Coefficients

Δt	$c^1_{l,max}$	Error^1	$t(c^1_{l,max})$	$c^2_{l,max}$	Error^2	$t(c^2_{l,max})$
0.04	0.0011635	–	0.88	0.00113649	–	0.92
0.02	0.00119218	–	0.92	0.00113227	–	0.92
0.01	0.0146167	–	7.45	0.0823751	–	7.31
0.005	0.136315	0.333685	6.365	0.271198	0.198802	6.29
0.0025	0.258605	0.211395	6.3025	0.381947	0.088053	5.755
0.00125	0.32374	0.14626	5.78375	0.438826	0.031174	5.7325
0.000625	0.367117	0.102883	5.77125	0.465565	0.004435	5.72

Table 2.9
Pressure Difference

Δt	Δp^1	Error^1	Δp^2	Error^2
0.04	-0.127816	0.012816	-0.127665	0.012665
0.02	-0.127547	0.012547	-0.127664	0.012664
0.01	-0.126691	0.011691	-0.115572	0.000572
0.005	-0.112033	0	-0.101175	0.003825
0.0025	-0.102725	0.002275	-0.105263	0
0.00125	-0.102771	0.002229	-0.1099	0
0.000625	-0.104269	0.000731	-0.111787	0

with both the defect and the correction step approximations giving relatively accurate prediction of its value, as well as the time when this value is achieved.

The lift coefficient is much more sensitive: both w_1 and w_2 approximate the maximal lift coefficient poorly, until the time step becomes sufficiently small. At $\Delta t = 0.005$ the approximations start to produce better results. At the next two refinements of the time step size, $\Delta t = 0.0025$ and $\Delta t = 0.00125$, the correction step predicts the maximal value of the lift coefficient much more accurately, than does the defect step approximation; the time when this value is achieved, is also closer to the reference value for the correction step approximation, than it is for the defect step approximation.

The pressure difference is also more accurately computed by the correction step approximation, with $\Delta p(8)$ inside the reference interval for $\Delta t \leq 0.0025$, whereas the defect step approximation produces the pressure difference outside of the reference interval for all values of Δt, except for $\Delta t = 0.005$.

2.5 Conclusion

In this chapter, a method was presented, that creates a turbulence model with reduced modeling error and reduced time discretization error. The method takes a model

of the newly proposed LES-C class and combines it with the deferred correction technique; this allows for the increased time accuracy for no extra computational cost, compared to the LES-C model. Following the Algorithm 2.1.1, this defect-deferred idea could be applied to any LES model. However, in this chapter only one model was considered, the Approximate Deconvolution Model (ADM). The application of Algorithm 2.1.1 with deferred correction for increased time accuracy, resulted in the ADC model. We were able to perform full numerical analysis for this model, including the proof of its stability and the error analysis. Four numerical tests were invoked to illustrate the model's performance, including the verification of claimed convergence rates, the flow past the step (2D and 3D) and the computation of drag and lift coefficients in the flow past the circular obstacle. In all these tests the correction step solution was shown to clearly outperform the defect solution - both qualitatively and quantitatively. This serves as a demonstration of the effectiveness of the ADC model, compared to the ADM: at least for the transitional flows in the chosen benchmark problems, the ADC solution gives higher accuracy per computational time, than the ADM solution. That is, the ADC could be used to either provide more accurate results than ADM on the same mesh; or the ADC could reach the same tolerance, as the ADM, while using a coarser mesh (in space and time) and obtaining the results faster.

Chapter 3

Grad-div Stabilization and 2D Flow around a Cylinder

3.1 Introduction

Grad-div stabilization has been a popular choice for solving the Stokes equation and NSE for low viscosity fluids and this technique is routinely used in various fluid flow applications, including turbulence modeling [24]. In [25, 26, 27, 28], it was shown that grad-div stabilization improves the accuracy and the convergence of iterative solvers of Stokes equation and NSE. It is shown in [29] that grad-div stabilization improves the stability and the accuracy of a solution to the Stokes equation. In [30]

a sensitivity analysis of the grad-div stabilization is performed on both the Stokes equation and NSE. A modular grad-div approach and its impact on the solution of the NSE is discussed in [31]. It also aims to improve the convergence of the iterative solvers.

The calculation of drag and lift coefficients around a cylindrical obstacle has been widely used as a quantitative benchmark problem for the NSE. High fidelity reference values for a direct numerical solution to the NSE are given in [2]. An earlier effort can be found in [32]. Similarly the drag and lift coefficients for the modular grad-div method were given [31]. However, there has been no detailed study of the impact of grad-div stabilization on drag and lift coefficients. In this chapter we use a series of numerical tests to suggest that grad-div stabilization can have an effect on the target quantities for this test problem. We further suggest a remedy making use of the Scott-Vogelius modified pressure, introduced in [33].

Scott-Vogelius finite elements, proposed in [34], produce a pointwise divergence-free solution to the Stokes equation or NSE. Scott-Vogelius finite elements achieve this using Lagrangian triangular elements, just as Taylor-Hood finite elements do, but also allowing a discontinuous pressure space. In this work, the Scott-Vogelius finite elements are only considered as a means of justifying our results, relying on the connection between grad-div stabilized Tayloor-Hood finite elements and Scott-Vogelius finite elements estabilished in [33]. In [33], it was shown that a Scott-Vogelius solution can be thought of as a limiting case of the stabilized Taylor-Hood solution.

Grad-div stabilized Taylor-Hood and Scott-Vogelius solutions for this problem was also considered in [35]. While this work showed that the grad-div stabilized Taylor-Hood calculations differ from the unstabilized case, it did not address how this may be corrected, or attempt to demonstrate that for large stabilization parameters the quantities of interest calculated with grad-div stabilized Taylor-Hood finite elements converge to those calculated with Scott-Vogelius finite elements.

3.2 Background

3.2.1 2D Incompressible Flow around a Cylinder

Returning to the benchmark problem outlined in chapter 1, we start by giving the definition of the drag and lift coefficients are given by:

$$c_d(t) = 20 \int_S \frac{\partial \mathbf{u_{ts}(t)}}{\partial n} n_y - p(t) n_x \, dS$$
$$c_l(t) = -20 \int_S \frac{\partial \mathbf{u_{ts}(t)}}{\partial n} n_x + p(t) n_x \, dS,$$

where $\mathbf{u_{ts}}$ is the velocity component tangential to the obstacle. As shown in[2], choosing a test function v_d such that $v_d = (1,0)^T$ on S and vanishes on all other boundaries and considering the weak form of the NSE, we can find an area integral over the whole domain for c_d. Likewise, we can choose $v_l = (0,1)^T$ on S, vanishing on other boundaries. These choices of test function give the following formulation for lift and drag coefficients:

$$c_d(t) = -20 \int_\Omega \nu \nabla u(t) : \nabla v_d + (u(t) \cdot \nabla) u(t) \cdot v_d - p(t)(\nabla \cdot v_d)\, dx\, dy$$
$$c_l(t) = -20 \int_\Omega \nu \nabla u(t) : \nabla v_l + (u(t) \cdot \nabla) u(t) \cdot v_l - p(t)(\nabla \cdot v_l)\, dx\, dy$$

However, grad-div stabilization introduces an extra term that we propose cannot be ignored. Thus, in the final numerical test we will also consider the formulae:

$$\bar{c}_d(t) = -20 \int_\Omega \nu \nabla u(t) : \nabla v_d + (u(t) \cdot \nabla) u(t) \cdot v_d - (p(t) - \gamma(\nabla \cdot u(t))(\nabla \cdot v_d)\, dx\, dy$$
$$\bar{c}_l(t) = -20 \int_\Omega \nu \nabla u(t) : \nabla v_l + (u(t) \cdot \nabla) u(t) \cdot v_l - (p(t) - \gamma(\nabla \cdot u(t))(\nabla \cdot v_l)\, dx\, dy$$

where $\bar{c}_d$ and $\bar{c}_l$ will be referred to as pressure-corrected drag and lift coefficients and γ is the grad-div stabilization parameter, discussed further in the next subsection.

3.2.2 Grad-Div Stabilization

The grad-div stabilization method is then obtained by adding $\gamma(\nabla\cdot u, \nabla\cdot v)$ to equation 1.2.2. We seek $(u, p) \in (X, Q)$ such that for all $(u, p) \in (X, Q)$:

$$(u_t, v) + (u \cdot \nabla u, v) - \nu(\nabla u, \nabla v) - (p, \nabla \cdot v) + \gamma(\nabla \cdot u, \nabla \cdot v) = (f, v)$$
$$(\nabla \cdot u, q) = 0 \qquad (3.2.1)$$

Since on the continuous level $\nabla \cdot u = 0$ pointwise, the term $\gamma(\nabla \cdot u, \nabla \cdot v) = 0$ for the continuous problem. In the discrete problem however, the stabilization term will serve to penalize solutions with poor mass conservation.

3.2.3 Modular Grad-Div Stabilization

The optimal grad-div parameter is problem dependent. For some time it was thought that most of the benefit of grad-div stabilization could be captured by $\gamma = O(1)$. However, in [33], it is suggested that large γ may be useful for some problems. For

large γ values, there may be breakdown of iterative solvers due to an increase in the condition number of corresponding linear system. As a remedy for those problems, the modular grad-div method was introduced in [31]. We considered the first of two algorithms proposed in that work. The following Algorithm is used along with the Crank-Nicolson time discretization. Note that two linear solves are required per time step, corresponding to step 1 and step 2.

Algorithm 3.2.1 *Step 1: Given $u^n \in X$, find $\hat{u}^{n+1} \in X$ and $p^{n+1} \in Q$ satisfying,*

$$(\frac{\hat{u}^{n+1} - u^n}{\Delta t}, v) + (u^n \cdot \nabla \hat{u}^{n+1}, v) + \nabla(p^{n+1}, v) = (f^{n+1}, v)$$

$$(\nabla \cdot \hat{u}^{n+1}, q) = 0$$

Step 2: Given $\hat{u}^{n+1} \in X$, find $u^{n+1} \in X$ satisfying,

$$(u^{n+1}, v) + (\beta + \gamma \Delta t)(\nabla \cdot u^{n+1}, \nabla \cdot v) = (\hat{u}^{n+1}, v) + \beta(\nabla \cdot u^n, \nabla \cdot v)$$

for all $v \in X$ and $q \in Q$

3.2.4 Scott-Vogelius Finite Element Spaces

We will also make use of the Scott-Vogelius finite element pair. Scott-Vogelius finite elements permit a discontinuous pressure space. This allows for very strict adherence

to the incompressibility condition. For example, take the $((P^2(\Omega)^2, P^1_{disc}(\Omega))$ spaces used in this work. Now, $\nabla \cdot u$ is an element of the pressure space. Thus, taking $q = \nabla \cdot u$ in 3.2.1, it is clear that the velocity field is pointwise divergence-free.

Ordinarily, when using Scott-Vogelius finite elements, one has to be careful not to violate the Ladyzhenskaya–Babuska–Brezzi (LBB^h) condition, also called the discrete inf-sup condition, given below as in [36].

Definition 3 (Ladyzhenskaya–Babuska–Brezzi Condition) *A velocity-pressure pair of spaces (X^h, Q^h) are said to satisfy the LBB^h condition if there exists β^h uniformly bounded away from 0 such that*

$$\inf_{q^h \in Q^h} \sup_{v^h \in X^h} \frac{(q^h, \nabla \cdot v^h)}{||v^h||||q^h||} \geq \beta^h > 0$$

where Q^h and X^h are finite dimensional subsets of Q and X and $||\cdot||$ represents the usual $L^2(\Omega)$ norm.

The difficulty arises from spurious pressure modes at singular nodes. Singular nodes are any node at the intersection of only two straight lines. However in [37] it was shown that the spaces $((P^k(\Omega)^2, P^{k-1}_{disc}(\Omega))$ satisfy the discrete LBB^h condition as long as 1) $k \geq d$ where $d = 2, 3$ is the dimension of the domain and 2) The mesh used is a barycenter refinement of a regular mesh. In particular, a mesh satisfying condition

2) cannot have singular nodes, leading to a much simpler implementation.

Since grad-div stabilization is a method for more tightly imposing mass conservation, it is natural to compare our results against Scott-Vogelius finite elements. Especially in light of [33], where it was proven that as $\gamma \to \infty$, the grad-div stabilized Taylor-Hood velocity converges to the Scott-Vogelius velocity. It was also shown that as $\gamma \to \infty$, $p_{TH} - \gamma(\nabla \cdot u_{TH}) \to p_{SV}$, where TH denotes a solution using Taylor-Hood finite elements and SV denotes the solution using Scott-Vogelius finite elements.

3.3 Numerical Tests and Results

In this section we present our numerical results and evaluate them by comparing them with the reference values. The reference interval given in [2] for the drag coefficient is $c_d \in [2.93; 2.97]$, for the lift coefficient is $c_l \in [0.47; 0.49]$, and for the pressure drop across the obstacle is $\Delta P \in [-0.115, -0.105]$. Crank-Nicolson time discretization was used in all simulations. A skew-symmetric form of the nonlinearity was used as well: $(u \cdot \nabla u, v) = \frac{1}{2}(u \cdot \nabla u, v) - \frac{1}{2}(u \cdot \nabla v, u)$ as is often done, see for example [24, 36]. All computations were done in FreeFEM++, see [19]. Our computations were done in two parts:

1. Compute the maximum drag coefficient, maximum lift coefficient, and final

pressure drop across the obstacle using equation 3.2.1 (grad-div stabilization) and algorithm 3.2.1 (modular grad-div stabilization) on a fixed mesh. Several γ values were used and for each γ a range of Δt was used from 0.04 to 0.0025. For algorithm 3.2.1, we take $\beta = \gamma$. For all of the calculations a fixed mesh with 65k velocity degree of freedom with 8k pressure degrees of freedom was used.

2. Compute the maximum drag, maximum lift, maximum pressure-corrected drag, and maximum pressure-corrected lift coefficients using grad-div stabilized Taylor-Hood finite elements on a barycenter refined mesh using a sufficiently small $\Delta t = 0.0025$. Then compare these results with the computed maximum drag and maximum lift coefficients on the same mesh using the same Δt and $((P^2(\Omega)^2, P^1_{disc}(\Omega))$ Scott-Vogelius finite elements. For these calculations, a fixed mesh with 64k velocity degrees of freedom with 48k discontinuous pressure degrees of freedom or 8k continuous pressure degrees of freedom was used. The mesh was generated using one barycenter refinement of a regular mesh.

3.3.1 Numerical Results for Standard and Modular grad-div Stabilization

The max drag coefficient calculation can be seen in the Table 1. All the values are within the reference range. For $\gamma = 0$ (the non stabilized case), the calculated max

drag coefficients are near to the middle of the reference range. Note also that for $\gamma = 0$ we recover maximum drag coefficient values very close to those in [2]. The same can be said for our results for maximal lift coefficient and final pressure drop discussed below. When grad-div stabilization is included, the max drag coefficient values are shifted toward the left endpoint of the reference interval. While the max drag coefficient decreases with increasing γ, the most notable impact comes from any nonzero choice of γ, causing a shift of 0.02 the coefficients. However, the max drag values do not depend significantly on Δt.

Table 3.1
Maximal Drag Coefficients using Standard Grad-div

Δt	$\gamma = 0$	$\gamma = 1$	$\gamma = 1000$	$\gamma = 100000$
0.04	2.95020	2.93960	2.93142	2.93117
0.02	2.95042	2.93986	2.93168	2.93143
0.01	2.95051	2.93995	2.93177	2.93153
0.005	2.95053	2.93997	2.93180	2.93155
0.0025	2.95053	2.93998	2.93180	2.93155

On the contrary, Table 2 shows that higher temporal accuracy is needed to capture the maximal lift coefficient, just as reported in [2]: The values are not within the reference interval until $\Delta t \leq 0.01$. In addition, the lift coefficient values are not as strongly dependent on γ as the maximal drag coefficient, but there is a consistent positive shift. In general we may wish to approximate lift coefficients to a very high accuracy and in those applications even a variation of $O(0.01)$ is significant. Thus, care should

be taken to acknowledge the small effect that grad-div stabilization introduces.

Table 3.2
Maximal Lift Coefficients using Standard Grad-div

Δt	$\gamma = 0$	$\gamma = 1$	$\gamma = 1000$	$\gamma = 100000$
0.04	0.377712	0.388797	0.389097	0.389069
0.02	0.446280	0.456438	0.456741	0.456709
0.01	0.468146	0.476338	0.476363	0.476330
0.005	0.472425	0.480351	0.480506	0.480474
0.0025	0.473326	0.481439	0.481519	0.481483

Of all three quantities of interest, ΔP depends on γ most weakly. From Table 3, it cannot be said that ΔP consistently increases or decreases with γ. However, it is still noteworthy that even for the most fine Δt the different γ values do not reach the same final pressure drop.

Table 3.3
ΔP Coefficients using Standard Grad-div

Δt	$\gamma = 0$	$\gamma = 1$	$\gamma = 1000$	$\gamma = 100000$
0.04	-0.102888	-0.102367	-0.102344	-0.102334
0.02	-0.106176	-0.107267	-0.107319	-0.107308
0.01	-0.110923	-0.111103	-0.111076	-0.111064
0.005	-0.111424	-0.111330	-0.111281	-0.111269
0.0025	-0.111607	-0.111447	-0.111607	-0.111380

For the modular grad-div calculations, we observe similar trends. In the Table 4, all the values are within the considered reference range. For $\gamma = 0$, the max drag coefficient values are in the middle of the reference range. But when modular grad-div stabilization was included, the max drag coefficient values are shifted to the left half

of the reference interval. Similarly to the grad-div calculation, the max drag values do not depend on Δt. There is a significant impact for nonzero γ, with the coefficient again decreasing slightly for even larger γ.

Table 3.4
Maximal Drag Coefficients using Modular Grad-div

Δt	$\gamma = 0$	$\gamma = 1$	$\gamma = 1000$	$\gamma = 100000$
0.04	2.95020	2.93780	2.93774	2.93775
0.02	2.95042	2.93804	2.93783	2.93778
0.01	2.95051	2.93818	2.93764	2.93763
0.005	2.95053	2.93825	2.93717	2.93717
0.0025	2.95053	2.93824	2.93634	2.93632

In the Table 5, the max lift coefficient calculation for the modular grad-div method can be observed. The observations are similar to the previous max lift coefficient calculation. Again, any nonzero γ produces a small rightward shift in the lift coefficient. As before, the maximum lift coefficient is sensitive to Δt.

Table 3.5
Maximal Lift Coefficients using Modular Grad-div

Δt	$\gamma = 0$	$\gamma = 1$	$\gamma = 1000$	$\gamma = 100000$
0.04	0.377712	0.378482	0.378587	0.378711
0.02	0.446280	0.447291	0.447477	0.447422
0.01	0.468146	0.471557	0.471863	0.471828
0.005	0.472425	0.477423	0.477880	0.478042
0.0025	0.473326	0.479629	0.480208	0.479900

In contrast to Table 3, we note that in Table 6, one detects a consistent shift in the final time pressure drop across the obstacle. As mentioned, modular grad-div stabilization

is a more stable method for large γ. The extra stability is likely what allows us to recover this small effect which was not seen using standard grad-div stabilization. While the positive shift is admittedly small for this problem, it should be noted that larger effects could be seen for other benchmark problems not considered in this work. Additionally, it is conceivable that even a change of O(0.0001) could be significant in some applications especially if, as these results may suggest, the effect is visible across a wide range of Δt values.

Referring now to all three quantities of interest, it would be interesting to investigate if the effect of standard/modular grad-div stabilization is diminished on a fine mesh or for sufficiently small Δt. While a more detailed study is needed, the data may already suggest that refining Δt is not enough to correct the discrepancy. If the effect is indeed resistant to increased computational effort, then using the pressure-corrected coefficients discussed in the next subsection may be unavoidable.

Table 3.6
ΔP Coefficients for Modular grad-div method with different γ

Δt	$\gamma = 0$	$\gamma = 1$	$\gamma = 1000$	$\gamma = 100000$
0.04	-0.102888	-0.102800	-0.102801	-0.102795
0.02	-0.106176	-0.106271	-0.106278	-0.106294
0.01	-0.110923	-0.110898	-0.110906	-0.110907
0.005	-0.111424	-0.111298	-0.111297	-0.111299
0.0025	-0.111607	-0.111429	-0.111404	-0.111404

3.3.2 Comparison between Grad-Div Stabilized Taylor-Hood and Scott-Vogelius Finite Elements

A comparison of the coefficients for the Scott-Vogelius (represented by SV in the last column) case as well as the pressure-corrected and uncorrected stabilized Taylor-Hood case is given in the following table. The results are presented for the finest $\Delta t = 0.0025$ value considered in this analysis, but similar results were seen for all Δt tested.

Table 3.7
Comparison of Corrected and Uncorrected Coefficients and the Scott-Vogelius Results

γ	1	100	100000	SV
c_d	2.93196	2.93189	2.93166	
c_l	0.486703	0.486886	0.486844	
$\bar{c}_d$	2.95000	2.95000	2.95000	2.95001
$\bar{c}_l$	0.487622	0.487811	0.487813	0.488330

One can see that the corrected drag coefficients are much closer to the center of the reference interval than the uncorrected values. The drag coefficient is known to be much less sensitive than the lift coefficient [2]. Thus it is unsurprising that convergence is achieved very quickly, essentially right away for $\gamma = 1$. On the other hand, the convergence for the corrected lift coefficient is slow. The nonlinear problem is difficult to solve for higher γ values, but perfect convergence is expected eventually.

3.4 Conclusion

We have shown that some care must be taken in applying grad-div stabilization to well-known test problems. First we have shown that for 2D flow around a cylinder, grad-div stabilization and modular grad-div stabilization has a consistent and nearly identical effect on the maximal drag coefficient, maximal lift coefficient, and pressure drop across the obstacle. Next we showed that this can be corrected for using a modified pressure, motivated by the relationship between Scott-Vogelius finite elements and grad-div stabilized Taylor-Hood finite elements.

It remains to be seen if grad-div stabilization has this effect on other test problems. If grad-div stabilization does have an impact on other benchmark problems, it may be of interest to investigate if a Scott-Vogelius modified pressure is applicable outside the analysis here.

Of course, how to select γ is still an open question. This analysis does not attempt to address the question, but may suggest as in [33] that for some problems a large γ could be required to achieve extremely high fidelity convergence to the reference value. Where necessary, one could investigate whether the modular grad-div stabilized NSE has the same relationship to the NSE solved with Scott-Vogelius finite elements and, if so, investigate if a modular grad-div stabilization plus Scott-Vogelius modified

pressure would allow for accurate results for high γ values.

Chapter 4

Note On Two Formulations of Crank-Nicolson Method for Navier-Stokes Equations

4.1 Introduction

In this short chapter we will discuss one further detail of implemening the NSE: the precise formulation of Crank-Nicolson method for time discretization, particularly with regards to pressure, and how that may affect results.

Discretizing equation 1.2.2 in time, we introduce the time step Δt, with $0 = t_0 < t_1 < t_2 < ... < t_N = T$, $\Delta t = t_{i+1} - t_i$, $\forall i = 0, 1, 2, ..., N-1$. The continuous in space, discrete in time models will be created, that seek approximations (u^i, p^i) to the true velocity-pressure pair $(u(t_i), p(t_i))$. In the numerical tests below the Taylor-Hood finite element method will accompany the Crank-Nicolson time discretization, to create a fully discrete formulation of (1.2.1). We will omit the detailed discussion of the spatial discretization, as it is not relevant to the topic of this report.

The Crank-Nicolson (CN) method, that is extremely popular among the researchers and practitioners, was first introduced in [38]. Since that time, it has been used in a plethora of applications; it has also been known for more than half a century, that the CN solutions could exhibit non-physical oscillatory behaviour, see, e.g., [39, 40]. Nevertheless, the method is still routinely used for many real-life applications, including fluid flow modeling. In the latter, there are some reports that suggest a combination of the CN with some other methods to overcome the instability issue - see, e.g., [41] and the references therein; however, there is also a large body of literature where the CN method is used for solving the NSE without any extra effort made to remove the possible oscillations, e.g., [1].

There are two well-known and widely used formulations of the Crank-Nicolson time discretization method for the NSE, that differ in the treatment of the pressure term. The first model, that we will denote by CN1, reads

$$\frac{u^{n+1}-u^n}{\Delta t} - \nu\Delta\left(\frac{u^{n+1}+u^n}{2}\right) + \left(\frac{u^{n+1}+u^n}{2}\right)\cdot\nabla\left(\frac{u^{n+1}+u^n}{2}\right) + \nabla p^{n+1} = \frac{f(t_{n+1})+f(t_n)}{2}. \tag{4.1.1}$$

This model has been widely used in various applications for more than thirty years; in particular, we want to mention that exactly this formulation of the Crank-Nicolson method was utilized in [2], where the drag and lift coefficients were computed for a flow around a circle.

Another formulation of the CN method, that we will denote here by CN2, has also been widely used for many years. It aims to create a second order accurate approximation for both velocity and pressure, and it reads

$$\frac{u^{n+1}-u^n}{\Delta t} - \nu\Delta\left(\frac{u^{n+1}+u^n}{2}\right) + \left(\frac{u^{n+1}+u^n}{2}\right)\cdot\nabla\left(\frac{u^{n+1}+u^n}{2}\right) + \nabla\left(\frac{p^{n+1}+p^n}{2}\right) = \frac{f(t_{n+1})+f(t_n)}{2}. \tag{4.1.2}$$

The purpose of this report is to apply these two models to a well-known test problem and show that the presumably more attractive model CN2 (which approximates the pressure with second order accuracy in time, whereas the model CN1 is only first order accurate in approximating the pressure) leads to a solution with poor quality and non-physical oscillations. On the contrary, the CN1 solution doesn't have oscillations and seems to be a much more attractive choice - at least for the test problem at hand. However, we will also show how to overcome the issues of the CN2 model: it is sufficient to use the time averaged solution $\frac{u^{n+1}+u^n}{2}$ of CN2, when computing the quantities of interest.

4.2 Numerical Test

4.2.1 Drag and Lift Coefficients

We will use two versions of the Crank-Nicolson method, combined with the Taylor-Hood (piecewise quadratic polynomials for velocity and piecewise linears for pressure) finite element method for spatial discretization, to model a flow past a circular obstacle, described in chapter 1.

Figure 4.1 below shows the evolution of the drag coefficient, computed for $0 \leq t \leq 8$. The maximal drag coefficient is compared against the results in [2], Table VI.

The number of degrees of freedom in our computations is $65,288$ d.o.f.s for velocity and $8,297$ d.o.f.s for pressure; this mesh is somewhere between Level 2 and Level 3 meshes, per the classification in [2]. The drag coefficient, computed (at time t_n) with the solution u^n of the model CN2, clearly exhibits nonphysical oscillations, and this model's prediction of the maximal value of drag is poor. To the contrary, when the CN1 model is used, the maximal value of the drag coefficient is very close to the one computed in [2] (2.9508 vs. 2.95089), and there are no nonphysical oscillations in the CN1 solution.

Another result that we report here, is the following. If one computes the drag at time t_n, using the CN1 solution u^n; then computes the drag at time $t_{n+1/2}$, using the CN2 solution $\frac{u^{n+1}+u^n}{2}$, and plots both $Drag(t)$ functions on one plot - the results are virtually indistinguishable. See the zoomed version of the plot, Figure 4.2, for a more noticeable difference in these solutions.

Similar to the situation with the drag coefficient, the (clearly nonphysical) oscillations are seen when a CN1 solution u^n is used to compute the time evolution of the pressure drop, $\Delta p(t) = p(t; 0.15, 0.2) - p(t; 0.25, 0.2)$. These oscillations disappear, if a CN2 solution u^n or a CN1 averaged solution $\frac{u^{n+1}+u^n}{2}$ is used instead - see Figures 4.3-4.4 below.

Finally, we look at the lift coefficient. As is shown in Figures 4.5-4.6, the models CN1 and CN2 provide comparable results in computing the evolution of the lift coefficients.

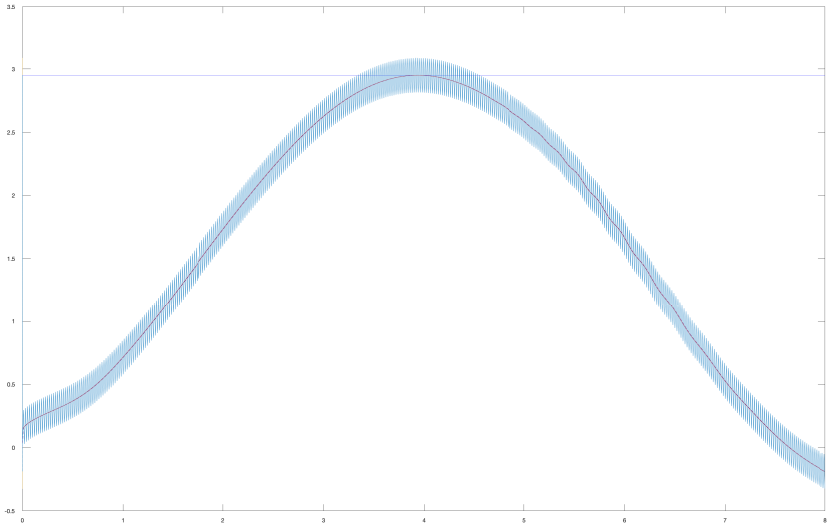

Figure 4.1: Evolution of the Drag Coefficient, computed with the CN2 solution (oscillatory) vs CN1 solution. Indistinguishable from the CN1 solution is the plot of the Drag Coefficient, computed with the averaged CN2 solution $\frac{u^{n+1}+u^n}{2}$. The horizontal line shows the maximal Drag Coefficient value of 2.9508.

4.3 Conclusion

We considered two formulations of the Crank-Nicolson method, CN1 and CN2, that differ in their treatment of the pressure term. Both models were applied to a test problem of flow past a circular obstacle. When calculating the drag coefficient and the pressure drop (difference of pressure in front of and past the obstacle), the CN2 solution showed nonphysical oscillations. This is especially interesting and frustrating to the researchers who would prefer to use the CN2 model: it could be viewed as more favorable than model CN1, because its a priori error estimates show that it

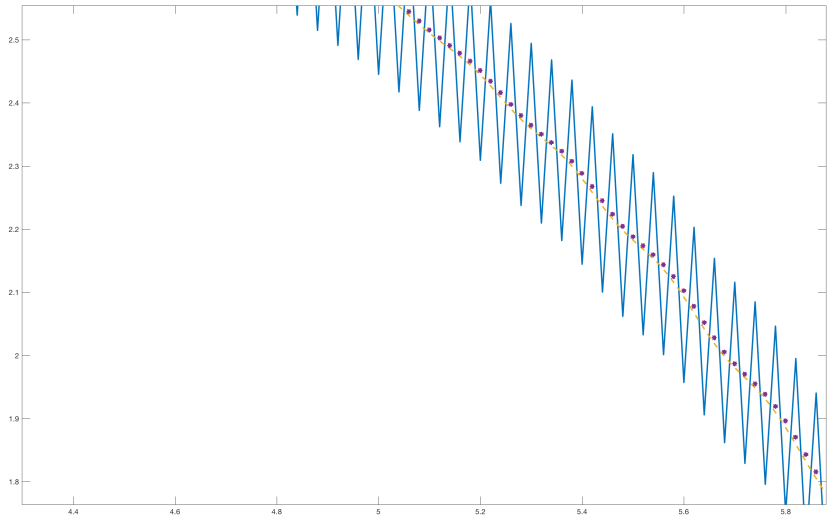

Figure 4.2: Evolution of the Drag Coefficient, Zoomed In. Here we notice the difference between drag coefficient computed with the CN1 solution u^n, and the drag coefficient computed with the averaged CN2 solution $\frac{u^{n+1}+u^n}{2}$.

approximates the pressure with second order accuracy w.r.t. the time step - whereas the CN1 model is only first order accurate in time. However, we also showed that, at least for this test problem, there is a simple "fix" that improves the quality of the CN2 solution and removes the nonphysical oscillations: the averaged solution $\frac{u^{n+1}+u^n}{2}$ should be used.

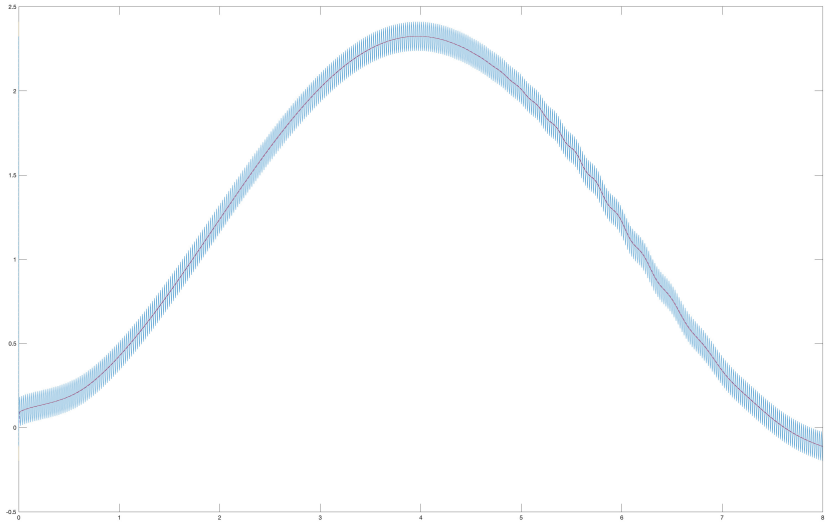

Figure 4.3: Evolution of the Pressure Drop $\Delta p(t) = p(t; 0.15, 0.2) - p(t; 0.25, 0.2)$, computed with the CN2 solution (oscillatory) vs CN1 solution. Indistinguishable from the CN1 solution is the plot of the Pressure Drop, computed with the averaged CN2 solution $\frac{u^{n+1}+u^n}{2}$.

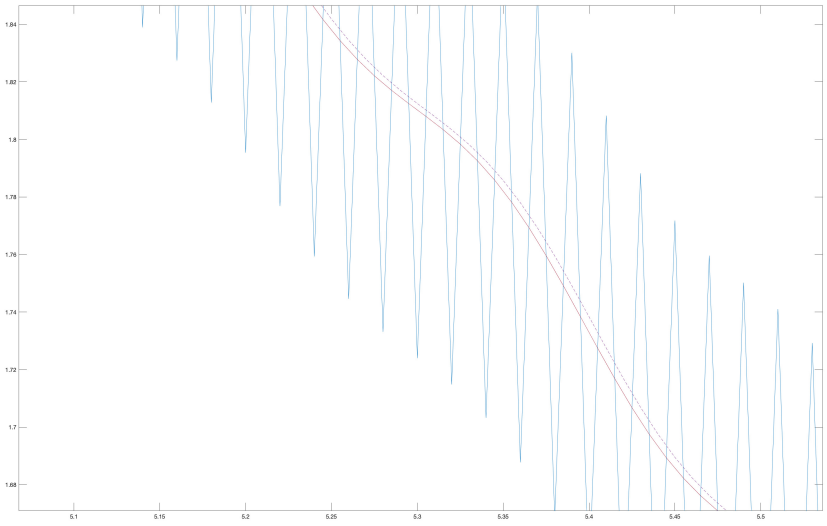

Figure 4.4: Evolution of the Pressure Drop, Zoomed In. Here we notice the difference between the pressure drop computed with the CN1 solution u^n (dashed), and the pressure drop computed with the averaged CN2 solution $\frac{u^{n+1}+u^n}{2}$.

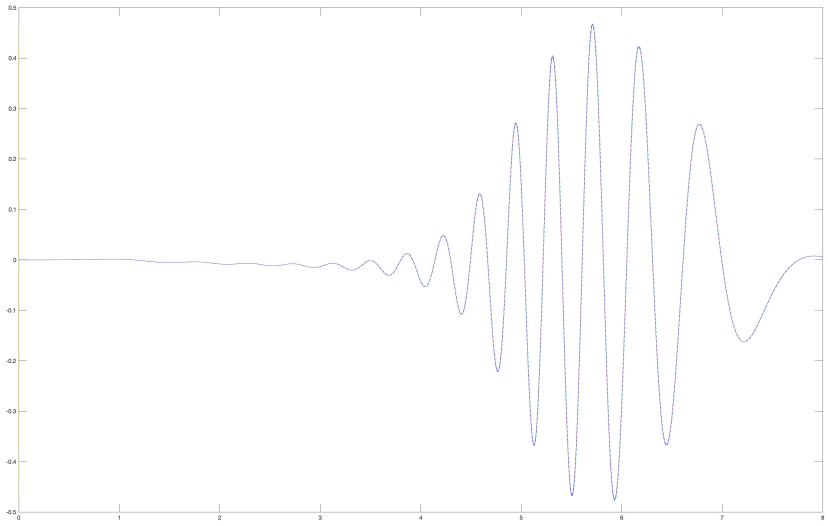

Figure 4.5: Evolution of the Lift Coefficient, computed with the CN2 solution, CN1 solution, and the averaged CN2 solution $\frac{u^{n+1}+u^n}{2}$. None of these solutions exhibit nonphysical oscillations.

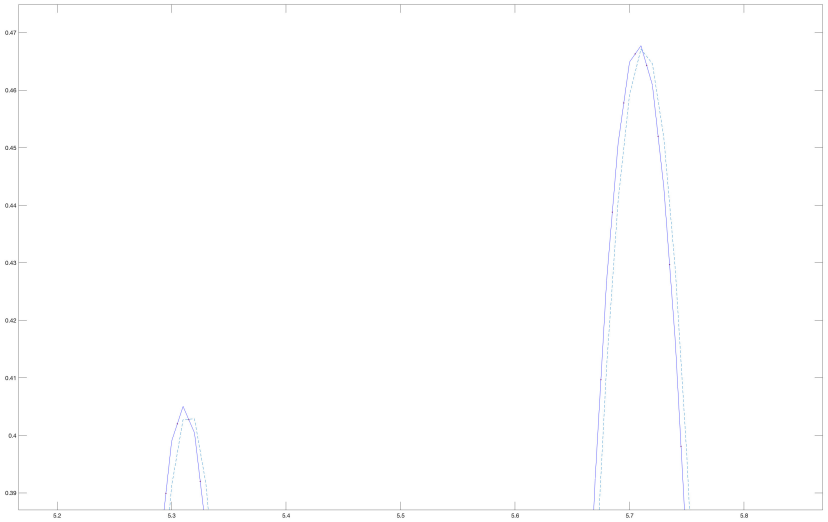

Figure 4.6: Evolution of the Lift Coefficient, Zoomed In. Here we notice the small difference between the three solutions (dashed solution of CN1, dots used to denote the average of the CN2 solution) from Figure 4.5.

References

[1] Labovsky, A. *SIAM J. Numer. Anal.* **2020**.

[2] John, V. *Numerical Methods in Fluids* **2004**, *44(7)*, 777–788.

[3] M, S.; S., T. In H., H. E., Ed., *Notes on Numerical Fluid Mechanics*, Vol. 52, pages 547–566. Vieweg: Braunschweig, 1996.

[4] Dutt, A.; Greengard, L.; Rokhlin, V. *BIT Numerical Mathematics* **2000**, *40*(2), 241–266.

[5] Minion, M. L. *Comm. Math. Sci.* **2003**, *1(3)*, 471–500.

[6] Minion, M. L. *Appl. Numer. Math.* **2004**, *48(3-4)*, 369–387.

[7] Gunzburger, M.; Labovsky, A. *M3AS: Mathematical Models and Methods in Applied Sciences* **2012**, *22(6)*.

[8] Aggul, M.; Kaya, S.; Labovsky, A. *Applied Mathematics and Computation* **2019**, *358*, 25–36.

[9] Erkmen, D.; Kaya, S.; Cibik, A. *Journal of Computational and Applied Mathematics* **2020**, *371*.

[10] Aggul, M.; Connors, J.; Erkmen, D.; Labovsky, A. *SIAM J. Numer. Anal.* **2018**, *56(4)*, 2484–2512.

[11] Erkmen, D.; Labovsky, A. *Journal of Mathematical Analysis and Applications* **2017**, *450*, 180–196.

[12] Aggul, M.; Labovsky, A. *Numerical Methods for Partial Differential Equations* **2017**, *33(3)*, 814–839.

[13] A. Bourlioux, A. T. Layton, M. L. M. *Journal of Computational Physics* **2003**, *189(2)*, 651–675.

[14] Connors, J.; Howell, J.; Layton, W. *SIAM Jour. Num. Analysis* **2012**, *50(3)*, 1297–1319.

[15] Dunca, A.; Epshteyn, Y. *SIAM J. Math. Anal.* **2006**, *37(6)*, 1890–1902.

[16] Girault, V.; Raviart, P. *Finite element approximation of the Navier-Stokes equations*, Vol. 749; Springer-Verlag, 1979.

[17] Heywood, J. G.; Rannacher, R. *SIAM J. Numer. Anal.* **1990**, *27(2)*, 353–384.

[18] Labovsky, A. *Numerical Methods for Partial Differential Equations* **2008**, *25(1)*, 1–25.

[19] Hecht, F. *J. Numer. Math.* **2012**, *20*(3-4), 251–265.

[20] Gunzburger, M. *Finite Element Methods for Viscous Incompressible Flows - A Guide to Theory, Practices, and Algorithms;* Academic Press, 1989.

[21] John, V.; Liakos, A. *Int. J. Numer. Meth. Fluids* **2006**, *50*, 713–731.

[22] Layton, W.; Manica, C.; Neda, M.; Rebholz, L. *N.M.P.D.E* **2008**, *24(2)*, 555–582.

[23] Layton, W.; Rebholz, L. *Approximate Deconvolution Models of Turbulence: Analysis, Phenomenology and Numerical Analysis;* Springer-Verlag Berlin Heidelberg, 2016.

[24] Batugedara, Y.; Labovsky, A. E.; Schwiebert, K. J. *Comput. Methods Appl. Mech. Engrg.* **2021**, *377*, 113696.

[25] Jenkins, E. W.; John, V.; Linke, A.; Rebholz, L. G. *Advanced Computational Mathematics* **2014**, *40*, 491–516.

[26] Olshanskii, M. A. *Comput. Meth. Appl. Mech. Eng.* **2002**, *191*, 5515–5536.

[27] Kobelkov, G. M. *Russ. J. Numer. Anal. Math. Model* **1995**, *10*, 33–40.

[28] Linke, A.; Rebholz, L. G. *Comput. Methods Appl. Mech. Engrg.* **2013**, *261-262*, 142–153.

[29] Olshanskii, M. A.; Reusken, A. *Math. Comp.* **2004**, *73*, 1699–1718.

[30] Neda, M.; Pahlevani, F.; Rebholz, L. G.; Waters, J. *Journal of Numerical Mathematics* **2016**, *24 (3)*, 491–516.

[31] Fiordilino, J. A.; Layton, W.; Rong, Y. *Computer Methods in Applied Mechanics and Engineering* **2017**.

[32] Schafer, M.; TureK, S. *Notes on Numerical Fluid Mechanics* **1996**, *52*, 547–566.

[33] Case, M. A.; Ervin, V. J.; Linke, A.; Rebholz, L. G. *SIAM Journal on Numerical Analysis* **2011**, *49*, 1461–1481.

[34] Scott, L. R.; Vogelius, M. *Mathematical modelling and numerical analysis* **1985**, pages 111–143.

[35] D'Agnillo, E. M.; Rebholz, L. G. *Contemporary Mathematics* **2013**, *586*, 143–151.

[36] Layton, W. *Introduction to the Numerical Analysis of Incompressible Viscous Flows;* SIAM, 2008.

[37] Guzmán, J.; Scott, L. R. *Math. Comput.* **2019**, *88*, 515–529.

[38] J. Crank, P. N. In *Proc. Camb. Phil. Soc.*, Vol. 43, pages 50–67, 1947.

[39] Keast, P.; Mitchell, A. R. *The Computer Journal* **1966**, *9*(1), 110–114.

[40] Duffy, D. *Wilmott* **2004**, *4*, 68–76.

[41] Jiang, N.; Kubacki, M.; Layton, W.; Moraiti, M.; Tran, H. *J. of Computational and Applied Mathematics* **2015**, *281*, 263–276.

[42] Gunzburger, M.; Labovsky, A. *Journal of Computational Mathematics* **2011**, *29*, 131–140.

[43] Labovsky, A.; Trenchea, C. *Journal of Mathematical Analysis and Applications* **2011**, *377*, 516–533.

[44] Labovsky, A.; Trenchea, C. *Numerical Functional Analysis and Optimization* **2010**, *31(12)*, 1362–1385.

[45] Labovsky, A.; Trenchea, C.; Wilson, N. *Computational Methods in Applied Mathematics* **2015**, *15(1)*, 97–110.

[46] Galdi, G. P. *Springer Tracts in Natural Philosophy* **1994**, *I*.

[47] W. Layton, H. K. Lee, J. P. *Applied Mathematics and Computation* **2002**, *129*, 1–19.

[48] Ascher, U. M.; Ruuth, S. J.; Wetton, B. T. R. *SIAM J. Num. Anal.* **1995**, *32(3)*.

[49] Fernández, M. *Numerische Mathematik* **2013**, *123*.

[50] Bernardi, C.; Rebollo, T. C.; Lewandowski, R.; Murat, F. *SIAM J. Numer. Anal.* **2002**, *40*(6), 2368–2394.

[51] Böhmer, K.; Hemker, P. W.; Stetter, H. J. In Böhmer, K., Stetter, H. J., Eds., *Defect Correction Methods. Theory and Applications*, pages 1–32. Springer Verlag, 1984.

[52] Bresch, D.; Koko, J. *Int. J. Appl. Math. Comput. Sci.* **2006**, *16*(4), 419–429.

[53] Ervin, V.; Lee, H. *Numerical Methods for Partial Differential Equations* **2006**, *22*, 145–164.

[54] Arndt, D.; Bangerth, W.; Blais, B.; Fehling, M.; Gassmöller, R.; Heister, T.; Heltai, L.; Köcher, U.; Kronbichler, M.; Maier, M.; Munch, P.; Pelteret, J.-P.; Proell, S.; Simon, K.; Turcksin, B.; Wells, D.; Zhang, J. *Journal of Numerical Mathematics* **2021, accepted for publication**.

[55] Bao, J.-W.; Wilczak, J. M.; Choi, J.-K.; Kantha, L. H. *Monthly Weather Rev.* **2000**, *128*, 2190–2210.

[56] Bryan, F. O.; Kauffman, B. G.; Large, W. G.; Gent, P. R. *Tech. Report NCAR/TN-424+STR, National Center for Atmosphere Research* **1996**.

[57] Perlin, N.; Skyllingstad, E. D.; Samelson, R. M.; Barbour, P. L. *J. Phys. Oceanography* **2007**, *37*, 2081–2093.

[58] Lions, J.-L.; Temam, R.; Wang, S. *Comput. Mech. Adv.* **1993**, *1*, 55–119.

[59] Lions, J.-L.; Temam, R.; Wang, S. *Comput. Mech. Adv.* **1993**, *1*, 55–119.

[60] Xie, X.; Wells, D.; Wang, Z.; Iliescu, T. *Computer Methods in Applied Mechanics and Engineering* **2017**, *313(1)*, 512–534.

[61] Lemarie, F.; Blayo, E.; Debreu, L. In *Procedia Comput. Sci.*, Vol. 51, pages 2066–2075, 2015.

[62] Layton, W.; Lewandowski, R. *Analysis and Applications* **2008**, *6(1)*, 23–49.

[63] Berselli, L.; Kim, T.-Y.; Rebholz, L. *Discrete and Continuous Dynamical Systems* **2016**, *21(4)*, 1027–1050.

[64] Labovsky, A. *Computational Methods in Applied Mathematics* **2009**, *9(2)*, 154–164.

[65] Mathew, J. In *Proceedings of the Combustion Institute*, Vol. 29(2), pages 1995–2000, 2002.

[66] Labovsky, A. *Numerical Methods for Partial Differential Equations* **2015**, pages 268–288.

[67] Stolz, S.; Adams, N. *Physics of Fluids* **1999**, *11(7)*, 1699.

[68] Aggul, M.; Eroglu, F.; Kaya, S.; Labovsky, A. *Computer Methods in Applied Mechanics and Engineering* **2020**, *365*.

[69] Gunzburger, M.; Labovsky, A. *SIAM-ASA J. Uncertainty Quantification* **2014**, *2(1)*, 82–105.

[70] John, V. *International Journal for Numerical Methods in Fluids* **2004**, *44*, 777–788.

[71] Hecht, F. *J. Numer. Math.* **2012**, *20*(3-4), 251–265.